

## Nitroxyl Radical Plus Hydroxylamine Pseudo Self-Exchange Reactions: Tunneling in Hydrogen Atom Transfer

Adam Wu,<sup>†</sup> Elizabeth A. Mader,<sup>†</sup> Ayan Datta,<sup>‡,§</sup> David A. Hrovat,<sup>‡</sup>  
Weston Thatcher Borden,<sup>\*,‡</sup> and James M. Mayer<sup>\*,†</sup>

Department of Chemistry, Campus Box 351700, University of Washington, Seattle, Washington 98195-1700, and Department of Chemistry and the Center for Advanced Scientific Computing and Modeling, University of North Texas, 1155 Union Circle, 305070, Denton, Texas 76203-5070

Received May 31, 2009; E-mail: borden@unt.edu; mayer@chem.washington.edu

**Abstract:** Bimolecular rate constants have been measured for reactions that involve hydrogen atom transfer (HAT) from hydroxylamines to nitroxyl radicals, using the stable radicals TEMPO<sup>•</sup> (2,2,6,6-tetramethylpiperidine-1-oxyl radical), 4-oxo-TEMPO<sup>•</sup> (2,2,6,6-tetramethyl-4-oxo-piperidine-1-oxyl radical), di-*tert*-butylnitroxyl (<sup>t</sup>Bu<sub>2</sub>NO<sup>•</sup>), and the hydroxylamines TEMPO-H, 4-oxo-TEMPO-H, 4-MeO-TEMPO-H (2,2,6,6-tetramethyl-*N*-hydroxy-4-methoxy-piperidine), and <sup>t</sup>Bu<sub>2</sub>NOH. The reactions have been monitored by UV–vis stopped-flow methods, using the different optical spectra of the nitroxyl radicals. The HAT reactions all have  $|\Delta G^\ddagger| \leq 1.4$  kcal mol<sup>-1</sup> and therefore are close to self-exchange reactions. The reaction of 4-oxo-TEMPO<sup>•</sup> + TEMPO-H → 4-oxo-TEMPO-H + TEMPO<sup>•</sup> occurs with  $k_{2H,MeCN} = 10 \pm 1$  M<sup>-1</sup> s<sup>-1</sup> in MeCN at 298 K ( $K_{2H,MeCN} = 4.5 \pm 1.8$ ). Surprisingly, the rate constant for the analogous deuterium atom transfer reaction is much slower:  $k_{2D,MeCN} = 0.44 \pm 0.05$  M<sup>-1</sup> s<sup>-1</sup> with  $k_{2H,MeCN}/k_{2D,MeCN} = 23 \pm 3$  at 298 K. The same large kinetic isotope effect (KIE) is found in CH<sub>2</sub>Cl<sub>2</sub>,  $23 \pm 4$ , suggesting that the large KIE is not caused by solvent dynamics or hydrogen bonding to solvent. The related reaction of 4-oxo-TEMPO<sup>•</sup> with 4-MeO-TEMPO-H(D) also has a large KIE,  $k_{3H}/k_{3D} = 21 \pm 3$  in MeCN. For these three reactions, the  $E_{aD} - E_{aH}$  values, between  $0.3 \pm 0.6$  and  $1.3 \pm 0.6$  kcal mol<sup>-1</sup>, and the  $\log(A_H/A_D)$  values, between  $0.5 \pm 0.7$  and  $1.1 \pm 0.6$ , indicate that hydrogen tunneling plays an important role. The related reaction of <sup>t</sup>Bu<sub>2</sub>NO<sup>•</sup> + TEMPO-H(D) in MeCN has a large KIE,  $16 \pm 3$  in MeCN, and very unusual isotopic activation parameters,  $E_{aD} - E_{aH} = -2.6 \pm 0.4$  and  $\log(A_H/A_D) = 3.1 \pm 0.6$ . Computational studies, using POLYRATE, also indicate substantial tunneling in the (CH<sub>3</sub>)<sub>2</sub>NO<sup>•</sup> + (CH<sub>3</sub>)<sub>2</sub>NOH model reaction for the experimental self-exchange processes. Additional calculations on TEMPO(<sup>•</sup>H), <sup>t</sup>Bu<sub>2</sub>NO(<sup>•</sup>H), and Ph<sub>2</sub>NO(<sup>•</sup>H) self-exchange reactions reveal why the phenyl groups make the last of these reactions several orders of magnitude faster than the first two. By inference, the calculations also suggest why tunneling appears to be more important in the self-exchange reactions of dialkylhydroxylamines than of arylhydroxylamines.

### Introduction

Hydrogen transfer reactions are among the most fundamental of chemical reactions.<sup>1</sup> Tunneling of the proton is emphasized in many treatments of hydrogen transfer,<sup>1–4</sup> and an increasing number of these reactions are being found to have large hydrogen/deuterium kinetic isotope effects (KIEs) and activation parameters that indicate the importance of

tunneling.<sup>5</sup> While a number of these reactions are understood in detail, there is limited intuition about why some hydrogen-transfer reactions display the hallmarks of tunneling and others do not. Described here are experimental and computational studies of hydrogen-atom transfer (HAT) pseudo self-exchange reactions between dialkylnitroxyl radicals and dialkylhydroxylamines (eq 1) that indicate the occurrence of substantial hydrogen tunneling. These are simple and unusual cases of tunneling in oxygen-to-oxygen HAT. The contrast between these reactions and the closely related reactions of arylnitroxyl radicals, which do not show the experimental markers of tunneling, is also examined.

<sup>†</sup> University of Washington.

<sup>‡</sup> University of North Texas.

<sup>§</sup> Current address: Indian Institute of Science Education and Research Thiruvananthapuram, CET Campus, Kerala-695016, India.

- (1) *Hydrogen-Transfer Reactions*; Hynes, J. T., Klinman, J. P., Limbach, H.-H., Schowen, R. L., Eds.; Wiley-VCH: Weinheim, 2007.
- (2) (a) Hammes-Schiffer, S. In *Hydrogen-Transfer Reactions*; Hynes, J. T., Klinman, J. P., Limbach, H.-H., Schowen, R. L., Eds.; Wiley-VCH: Weinheim, 2007; Vol. 2, pp 479–502. (b) Fernandez-Ramos, A.; Ellingson, B. A.; Garrett, B. C.; Truhlar, D. G. In *Reviews in Computational Chemistry*; Cundari, T. R., Lipkowitz, K. B., Eds.; Wiley-VCH: Hoboken, NJ, 2007; Vol. 23, pp 125–232.
- (3) Bell, R. P. *The Tunnel Effect in Chemistry*; Chapman and Hall: London, 1980; pp 77–105.
- (4) Carpenter, B. K. *Determination of Organic Reaction Mechanisms*; John Wiley & Sons: New York, 1984; pp 83–111.

- (5) See, for example: (a) Klinman, J. P. *Phil. Trans. R. Soc. B* **2006**, *361*, 1323. (b) Sutcliffe, M. J.; Masgrau, L.; Roujeinikova, A.; Johannissen, L. O.; Hothi, P.; Basran, J.; Ranaghan, K. E.; Mulholland, A. J.; Leys, D.; Scrutton, N. S. *Phil. Trans. R. Soc. B* **2006**, *361*, 1375. (c) Barroso, M.; Arnaut, L. G.; Formosinho, S. J. *J. Phys. Org. Chem.* **2009**, *22*, 254–263. (d) Meyer, T. J.; Huynh, M. H. V. *Inorg. Chem.* **2003**, *42*, 8140–8160. (e) Reinaud, O. M.; Theopold, K. H. *J. Am. Chem. Soc.* **1994**, *116*, 6979–6980. (f) Mahapatra, S.; Halfen, J. A.; Tolman, W. B. *J. Am. Chem. Soc.* **1996**, *118*, 11575–11586. (g) Zheng, H.; Lipscomb, J. D. *Biochemistry* **2006**, *45*, 1685–1692.



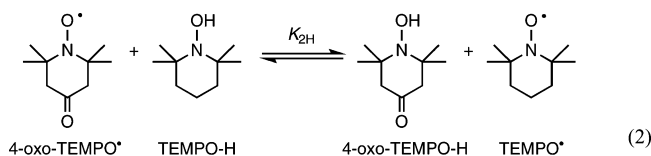
Hydrogen atom transfer (HAT) has been studied for over a century<sup>6</sup> and is the simplest chemical reaction that involves the transfer of two particles, a proton and an electron. It can therefore be considered to be a type of “proton-coupled electron transfer” (PCET).<sup>7,8</sup> HAT is important in combustion and selective oxidation of alkanes, in the formation and reactivity of protein-based radicals and reactive oxygen species (ROS), and many other processes.<sup>9</sup> For example, HAT from the double allylic C–H bond in linoleic acid to the iron(III)-hydroxide active site in lipoxygenases has received particular attention because its H/D KIE of up to ~80 indicates the importance of tunneling.<sup>5a,10</sup> HAT involving nitroxyl radicals and hydroxylamines is important in much of the chemistry of nitroxyl radicals,<sup>11</sup> such as their role as catalysts and cocatalysts in oxidation of organic substrates.<sup>12–15</sup> *N*-hydroxyphthalimide (NHPI) has been widely explored as a cocatalyst in Co/Mn-catalyzed autoxidations of alkylaromatics, with the active species being the corresponding phthalimide *N*-oxyl radical (PINO<sup>•</sup>).<sup>16</sup> HAT reactions from benzylic C–H bonds to PINO<sup>•</sup> in acetic acid have large deuterium KIEs (17–28 at 298 K)<sup>17</sup> and the

pseudo self-exchange reaction between PINO<sup>•</sup> and 4-Me-NHPI in acetic acid has  $k_{\text{H}}/k_{\text{D}} = 11.0$  ( $k_{\text{H}} = 677 \pm 24 \text{ M}^{-1} \text{ s}^{-1}$ ).<sup>18</sup> Reactions of nitroxyl radicals with arylhydroxylamines, however, exhibit much smaller KIEs, with  $k_{\text{H}}/k_{\text{D}} = 1.5–1.9$  at ambient temperatures (see Table 2 below).<sup>13,14</sup>

We have focused on HAT self-exchange reactions, such as the nitroxyl/hydroxylamine reactions examined here (eq 1), both because of their relative simplicity and because of our finding that the Marcus cross relation usually predicts HAT rate constants within an order of magnitude or two.<sup>19–21</sup> This treatment is a new approach to understanding HAT rate constants<sup>22</sup> and has been found to hold for both organic reactions and examples involving transition metal complexes. For instance, the cross relation predicts and explains the inverse temperature dependence of the rate of HAT from  $[\text{Fe}^{\text{II}}(\text{H}_2\text{bip})_3]^{2+}$  to the stable nitroxyl radical TEMPO<sup>•</sup> (2,2,6,6-tetramethylpiperidine-1-oxyl radical).<sup>20</sup> Of the various HAT reactions involving TEMPO<sup>•</sup>/TEMPO-H and transition metal complexes that we have examined,<sup>19,20,23,24</sup> the Marcus approach appears to be least accurate for  $\text{Ru}^{\text{II}}(\text{acac})_2(\text{py-imH}) + \text{TEMPO}^\bullet \rightarrow \text{TEMPO-H}$  and  $\text{Ru}^{\text{III}}(\text{acac})_2(\text{py-im})$ , which has a large KIE.<sup>24b</sup> These results prompted our examination of nitroxyl/hydroxylamine self-exchange reactions; the kinetics of 4-oxo-TEMPO<sup>•</sup> plus TEMPO-H were briefly mentioned in a preliminary communication about the  $[\text{Fe}^{\text{II}}(\text{H}_2\text{bip})_3]^{2+}$  reaction.<sup>20</sup>

## Results

**I. Equilibrium Constants.** The reaction of 4-oxo-TEMPO<sup>•</sup> and TEMPO-H in CD<sub>3</sub>CN forms an equilibrium mixture with 4-oxo-TEMPO-H and TEMPO<sup>•</sup> (eq 2), with all four species observed by <sup>1</sup>H NMR spectroscopy. All of the resonances have been assigned for the paramagnetic and diamagnetic species,



even though 4-oxo-TEMPO-H has not been isolated. Equilibrium is rapidly established (see below) and integration of each species using Lorentzian line fitting gave  $K_{2\text{H,CD}_3\text{CN}} = 4.5 \pm$

- (6) Kochi, J. K. *Free Radicals*; Wiley: New York, 1973.  
 (7) (a) Huynh, M. H. V.; Meyer, T. J. *Chem. Rev.* **2007**, *107*, 5004. (b) Meyer, T. J.; Huynh, M. H. V. *Inorg. Chem.* **2003**, *42*, 8140. (c) Hodgkiss, J. M.; Rosenthal, J.; Nocera, D. G. In *Hydrogen-Transfer Reactions*; Hynes, J. T.; Klinman, J. P.; Limbach, H.-H.; Schowen, R. L. Eds.; Wiley-VCH: Weinheim, 2007; Volume 2, pp 503–562. (d) Stubbe, J.; Nocera, D. G.; Yee, C. S.; Chang, M. C. Y. *Chem. Rev.* **2003**, *103*, 2167. (e) Cukier, R. I.; Nocera, D. G. *Annu. Rev. Phys. Chem.* **1998**, *49*, 337. (f) Partenheimer, W. *Catal. Today* **1995**, *23*, 69.  
 (8) (a) Mayer, J. M. *Annu. Rev. Phys. Chem.* **2004**, *55*, 363. (b) Mayer, J. M.; Rhile, I. J. *Biochim. Biophys. Acta* **2004**, *1655*, 51. (c) Mayer, J. M.; Rhile, I. J.; Larsen, F. B.; Mader, E. A.; Markle, T. F.; DiPasquale, A. G. *Photosynth. Res.* **2006**, *87*, 3. (d) Mayer, J. M.; Mader, E. A.; Roth, J. P.; Bryant, J. R.; Matsuo, T.; Dehestani, A.; Bales, B. C.; Watson, E. J.; Osako, T.; Valliant-Saunders, K.; Lam, W.-H.; Hrovat, D. A.; Borden, W. T.; Davidson, E. R. *J. Mol. Catal. A: Chem.* **2006**, *251*, 24.  
 (9) (a) Knapp, M. J.; Meyer, M.; Klinman, J. P. In *Hydrogen-Transfer Reactions*; Hynes, J. T.; Klinman, J. P.; Limbach, H.-H.; Schowen, R. L., Eds.; Wiley-VCH: Weinheim, 2007; Volume 4, pp 1241–1284. (b) Stubbe, J.; van der Donk, W. A. *Chem. Rev.* **1998**, *98*, 705. (c) Halliwell, B.; Gutteridge, J. M. C. *Free Radicals in Biology and Medicine*; Oxford University Press: Oxford, 1999.  
 (10) (a) Knapp, M. J.; Rickert, K.; Klinman, J. P. *J. Am. Chem. Soc.* **2002**, *124*, 3865. (b) Lewis, E. R.; Johansen, E.; Holman, T. R. *J. Am. Chem. Soc.* **1999**, *121*, 1395.  
 (11) Likhtenshtein, G.; Yamauchi, J.; Nakatsuji, S.; Smirnov, A. I. *Nitroxides: Applications in Chemistry, Biomedicine, and Materials Science*; Wiley-VCH: New York, 2008.  
 (12) (a) Sheldon, R. A.; Arends, I. W. C. E. *J. Mol. Catal. A: Chem.* **2006**, *251*, 200. (b) Sheldon, R. A.; Arends, I. W. C. E. *Adv. Synth. Catal.* **2004**, *346*, 1051. (c) Sheldon, R. A.; Arends, I. W. C. E.; Brink, G.-J. T.; Dijkstra, A. *Acc. Chem. Res.* **2002**, *35*, 774. (d) For other applications of nitroxyl radicals, see refs 5–20 in: Vasbinder, M. J.; Bakac, A. *Inorg. Chem.* **2007**, *46*, 2322.  
 (13) (a) Kreilick, R. W.; Weissman, S. I. *J. Am. Chem. Soc.* **1966**, *88*, 2645. (b) Arick, M. R.; Weissman, S. I. *J. Am. Chem. Soc.* **1968**, *90*, 1654.  
 (14) (a) Malievskii, A. D.; Shapiro, A. B. *Kinet. Catal.* **2005**, *46*, 472. (b) Malievskii, A. D.; Koroteev, S. V.; Shapiro, A. B. *Kinet. Catal.* **2005**, *46*, 812. (c) Malievskii, A. D.; Koroteev, S. V.; Gorbunova, N. V.; Brin, E. F. *Kinet. Catal.* **1997**, *38*, 485.  
 (15) Dijkstra, A.; Marino-González, A.; Mairata i Payeras, A.; Arends, I. W. C. E.; Sheldon, R. A. *J. Am. Chem. Soc.* **2001**, *123*, 6826.  
 (16) Ishii, Y.; Sakaguchi, S.; Iwahama, T. *Adv. Synth. Catal.* **2001**, *343*, 393.  
 (17) (a) Koshino, N.; Saha, B.; Espenson, J. H. *J. Org. Chem.* **2003**, *68*, 9364. (b) Koshino, N.; Cai, Y.; Espenson, J. H. *J. Phys. Chem. A* **2003**, *107*, 4262. (c) Amorati, R.; Lucarini, M.; Mugnaini, V.; Pedulli, G. F. *J. Org. Chem.* **2003**, *68*, 1747.

- (18) Cai, Y.; Koshino, N.; Saha, B.; Espenson, J. H. *J. Org. Chem.* **2005**, *70*, 238.  
 (19) Roth, J. P.; Yoder, J. C.; Won, T.-J.; Mayer, J. M. *Science* **2001**, *294*, 2524.  
 (20) Mader, E. A.; Larsen, A. S.; Mayer, J. M. *J. Am. Chem. Soc.* **2004**, *126*, 8066.  $\text{H}_2\text{bip} = 2,2'$ -bi-1,4,5,6-tetrahydropyrimidine.  
 (21) Warren, J. J.; Mayer, J. M. manuscript in preparation.  
 (22) HAT rate constants have traditionally been analyzed using a correlation of Arrhenius activation energy  $E_a$  with enthalpic driving force  $\Delta H$  (the Bell-Evans-Polanyi relation), together with “polar effects” and other influences. (a) Ingold, K. U. In *Free Radicals*; Kochi, J. K., Ed.; Wiley: New York, 1973; Volume 1, p 69ff. (b) Russel, G. A. In *Free Radicals*; Kochi, J. K., Ed.; Wiley: New York, 1973; Volume 1, pp 275–331. (c) O’Neal, H. E.; Benson, S. W. In *Free Radicals*; Kochi, J. K., Ed.; Wiley: New York, 1973; Volume 2, p 302ff. (d) Tedder, J. M. *Angew. Chem., Int. Ed. Engl.* **1982**, *21*, 401.  
 (23) (a) Mader, E. A.; Davidson, E. R.; Mayer, J. M. *J. Am. Chem. Soc.* **2007**, *129*, 5153. (b) Mader, E. A.; Manner, V. W.; Markle, T. F.; Wu, A.; Franz, J. A.; Mayer, J. M. *J. Am. Chem. Soc.* **2009**, *131*, 4335–4345.  
 (24) acac = 2,4-pentanedionato; py-imH = 2-(2'-pyridyl)imidazole. (a) Wu, A.; Masland, J.; Swartz, R. D.; Kaminsky, W.; Mayer, J. M. *Inorg. Chem.* **2007**, *46*, 11190. (b) Wu, A.; Mayer, J. M. *J. Am. Chem. Soc.* **2008**, *130*, 14745–14754.





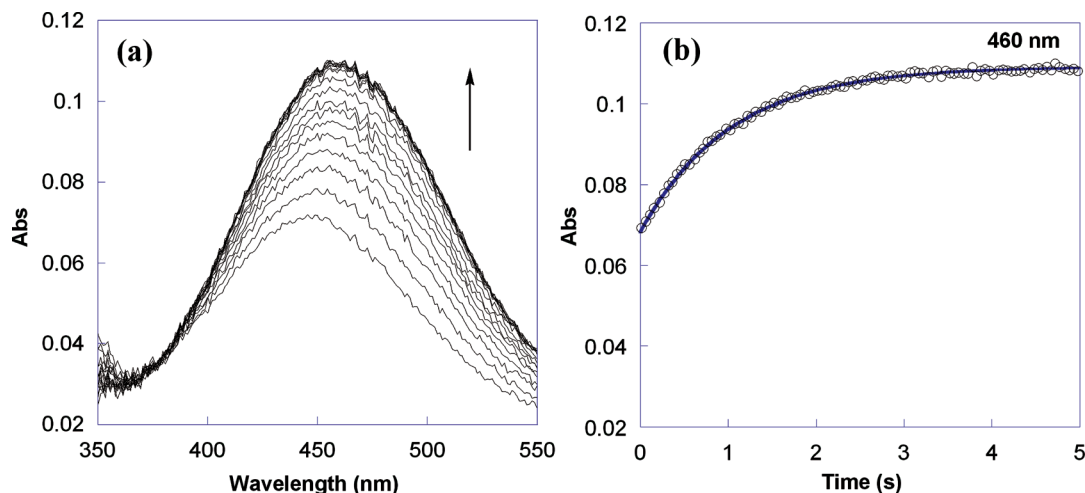


**Figure 2.** (a) Overlay of UV-vis spectra for the reaction of 8.8 mM 4-oxo-TEMPO\* with 88 mM TEMPO-H (eq 2) in MeCN over 5 s at 298 K. (b) Absorbance at 460 nm showing the raw data (o) and first order A  $\rightarrow$  B fit using SPECFIT (—).

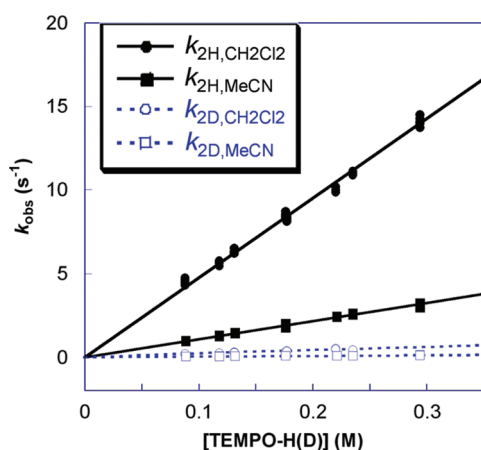


**Figure 3.** Plot of pseudo first order  $k_{\text{obs}}$  versus [TEMPO-H(D)] for reaction 2 in MeCN ( $k_{\text{H}}/k_{\text{D}} = 23 \pm 3$ ) and in  $\text{CH}_2\text{Cl}_2$  ( $k_{\text{H}}/k_{\text{D}} = 23 \pm 4$ ) at 298 K.

$\text{D}_2\text{O}$ . This TEMPO-D, which was  $98 \pm 1\%$  D by  $^1\text{H}$  NMR integration, reacts with 4-oxo-TEMPO\* in MeCN with  $k_{2\text{D,MeCN}} = 0.44 \pm 0.05 \text{ M}^{-1} \text{ s}^{-1}$  (Figure 3). This rate constant is  $23 \pm 3$  times slower than that for the same reaction of TEMPO-H at 298 K. Within experimental error, essentially the same apparent isotope effects are found in  $\text{CH}_2\text{Cl}_2$ ,  $23 \pm 4$ , and in  $\text{CCl}_4$ ,  $18 \pm 5$ . Thus solvent polarity and hydrogen bonding to solvent do not significantly affect the KIEs. The ratio of the rate constants, however, is only a lower limit to the true KIE because the residual  $2 \pm 1\%$  H in the TEMPO-D contributes significantly to the reactions. If the TEMPO-D was 99% D, the true KIE would be 30, and if it was 97% D, the true KIE would be 72.<sup>29</sup> These are the experimental bounds on the KIE.

The kinetics of 4-oxo-TEMPO\* plus excess 4-MeO-TEMPO-H (eq 3) in MeCN were measured and analyzed in a similar fashion, to give  $k_{3\text{H}} = 7.8 \pm 0.7 \text{ M}^{-1} \text{ s}^{-1}$  at 298 K (Figure S2, Supporting Information). This is about 20% lower than the rate constant for reaction 2 under the same conditions, which is consistent with the equilibrium constant for reaction 3,  $K_{3\text{H,MeCN}}$

$= 2.8 \pm 1.2$ , being a little smaller than  $K_{2\text{H,MeCN}} = 4.5 \pm 1.8$  for reaction 2.

Similar to the case for reaction 2, the rate constant for reaction of the deuterated hydroxylamine, 4-MeO-TEMPO-D, at 298 K is much slower,  $k_{3\text{D}} = 0.37 \pm 0.05 \text{ M}^{-1} \text{ s}^{-1}$  (Figure S2, Supporting Information), than that for the reaction of the undeuterated compound. Since the 4-MeO-TEMPO-D is also  $98 \pm 1\%$  deuterated, the  $k_{3\text{H}}/k_{3\text{D}} = 21 \pm 3$  at 298 K is also a lower limit to the true KIE. Rate constants and  $k_{\text{H}}/k_{\text{D}}$  values at 298 K for the forward reactions 2–4 are given in Table 2, along with the rate constants for other nitroxyl plus hydroxylamine reactions.

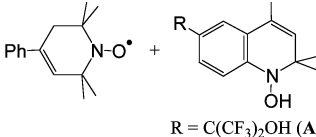
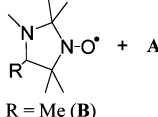
The reaction of  ${}^t\text{Bu}_2\text{NO}^*$  and TEMPO-H (eq 4) in MeCN is uphill in free energy ( $K_{4\text{H,MeCN}} = 0.11$ ), so the kinetics were measured by UV-vis stopped flow techniques under second order approach-to-equilibrium conditions. The optical spectra of  ${}^t\text{Bu}_2\text{NO}^*$  ( $\lambda_{\text{max}} = 454 \text{ nm}$ ,  $\epsilon = 8.9 \text{ M}^{-1} \text{ cm}^{-1}$ ) and TEMPO\* ( $\lambda_{\text{max}} = 460 \text{ nm}$ ,  $\epsilon = 10.3 \text{ M}^{-1} \text{ cm}^{-1}$ ) are similar, so the overall change of the absorbance is small (Figure S3, Supporting Information). Under the experimental conditions ( $[{}^t\text{Bu}_2\text{NO}^*] = 12\text{--}139 \text{ mM}$ ,  $[\text{TEMPO-H}] = 118\text{--}237 \text{ mM}$ ), spectra of reaction mixtures at short times show absorbances  $\sim 10\%$  higher than equimolar solutions of  ${}^t\text{Bu}_2\text{NO}^*$ , suggesting partial formation of a complex between  ${}^t\text{Bu}_2\text{NO}^*$  and TEMPO-H. Consistent with this suggestion, adding 2,4,6-tri-*tert*-butylphenol to solutions of  ${}^t\text{Bu}_2\text{NO}^*$  caused similar changes in optical spectra, even though HAT does not occur ( $\Delta\text{BDE} = +14 \text{ kcal mol}^{-1}$ ).<sup>30</sup> These changes in reaction 4 are subtle, however, and are too small to enable determination of a value for the equilibrium constant. There are also subtle differences between the final reaction spectrum and that of TEMPO\*, suggesting that the products could also be, in part, hydrogen-bonded.

The forward bimolecular rate constant for eq 4 under these conditions,  $k_{4\text{H,MeCN}}$ , is  $1.9 \pm 0.2 \text{ M}^{-1} \text{ s}^{-1}$  at 298 K, as determined by fitting the data to an opposing second order equilibrium model ( $\text{A} + \text{B} \rightleftharpoons \text{C} + \text{D}$ ) with a fixed  $K_{4\text{H,MeCN}} = 0.11$ , using SPECFIT<sup>28</sup> (Figure S3, Supporting Information). When TEMPO-D is used, the initial spectra of the reaction mixtures are much closer to those of solutions of pure  ${}^t\text{Bu}_2\text{NO}^*$ , suggesting that adduct formation is isotopically sensitive, and is less favorable for TEMPO-D than for

(29) The “true”  $k_{\text{H}}/k_{\text{D}}$ , at complete deuteration, is equal to  $\chi(\text{D})/[(k_{\text{H}}/k_{\text{D}})_{\text{obs}}^{-1} - \chi(\text{H})]$ , where  $\chi(\text{H})$  and  $\chi(\text{D})$  are the mole-fraction in H and D, respectively. For a discussion of the residual protio effect on the observed  $k_{\text{H}}/k_{\text{D}}$ , see: Sorokin, A.; Robert, A.; Meunier, B. *J. Am. Chem. Soc.* **1993**, *115*, 7293.

(30) BDE: 2,4,6-tri-*tert*-butylphenol ( $82.3 \text{ kcal mol}^{-1}$ ) and  ${}^t\text{Bu}_2\text{NOH}$  ( $68.2 \text{ kcal mol}^{-1}$ ).<sup>26</sup>

**Table 2.** Driving Forces, Rate Constants, and Kinetic Isotope Effects for Nitroxyl Plus Hydroxylamine Reactions<sup>a</sup>

Reaction	Solvent	$\Delta G^{\circ b}$	$k_H$ (M <sup>-1</sup> s <sup>-1</sup> ) <sup>a</sup>	$k_D$ (M <sup>-1</sup> s <sup>-1</sup> ) <sup>a,c</sup>	$k_H/k_D$ <sup>a,c</sup>	Ref.
4-oxo-TEMPO <sup>•</sup> + TEMPO-H <sup>d</sup>	MeCN	-0.9 ± 0.2	10 ± 1	0.44 ± 0.05	23 ± 3	<sup>e</sup>
4-oxo-TEMPO <sup>•</sup> + TEMPO-H	CH <sub>2</sub> Cl <sub>2</sub>	-1.2 ± 0.2	48 ± 4	2.1 ± 0.3	23 ± 4	<sup>e</sup>
4-oxo-TEMPO <sup>•</sup> + TEMPO-H	CCl <sub>4</sub>	–	300 ± 30	17 ± 4	18 ± 5	<sup>e</sup>
4-oxo-TEMPO <sup>•</sup> + 4-MeO-TEMPO-H	MeCN	-0.6 ± 0.2	7.8 ± 0.7	0.37 ± 0.05	21 ± 3	<sup>e</sup>
<sup>t</sup> Bu <sub>2</sub> NO <sup>•</sup> + TEMPO-H	MeCN	1.3 ± 0.2	1.9 ± 0.2	0.12 ± 0.02	16 ± 3	<sup>e</sup>
<sup>t</sup> Bu <sub>2</sub> NO <sup>•</sup> + TEMPO-H	CH <sub>2</sub> Cl <sub>2</sub>	1.4 ± 0.2	4.6 ± 0.4	0.35 ± 0.04	13 ± 2	<sup>e</sup>
PINO <sup>•</sup> + 4Me-NHPI <sup>f</sup>	AcOH(D)	-0.4 ± 0.1	677 ± 24	61.3 ± 2.1	11.0 ± 0.5	18
4-Me-PINO <sup>•</sup> + NHPI <sup>f</sup>	AcOH(D)	0.4 ± 0.1	354 ± 23	31.8 ± 2.0	11.1 ± 1.0	18
<sup>t</sup> Bu <sub>2</sub> NO <sup>•</sup> + <sup>t</sup> Bu <sub>2</sub> NOH	CCl <sub>4</sub>	0	320 ± 40	–	–	13
<sup>t</sup> Bu <sub>2</sub> NO <sup>•</sup> + <sup>t</sup> Bu <sub>2</sub> NOH	C <sub>6</sub> H <sub>5</sub> Cl	0	240 ± 60	–	–	13
<sup>t</sup> Bu(Ar)NO <sup>•</sup> + <sup>t</sup> Bu(Ar)NOH <sup>g</sup>	CCl <sub>4</sub>	0	(2.0 ± 0.4) × 10 <sup>3</sup>	(1.3 ± 0.2) × 10 <sup>3</sup>	1.5 ± 0.4	13
<sup>t</sup> Bu(Ar)NO <sup>•</sup> + <sup>t</sup> Bu(Ar)NOH <sup>g</sup>	C <sub>6</sub> H <sub>5</sub> Cl	0	(5.2 ± 0.4) × 10 <sup>2</sup>	–	–	13
<sup>t</sup> Bu(Ar)NO <sup>•</sup> + <sup>t</sup> Bu(Ar)NOH <sup>g</sup>	CH <sub>2</sub> Cl <sub>2</sub>	0	< 20	–	–	13
Ph <sub>2</sub> NO <sup>•</sup> + Ph <sub>2</sub> NOH	CCl <sub>4</sub>	0	> 10 <sup>7</sup>	–	–	13
	hexane	-0.2 ± 0.1	(4.3 ± 0.2) × 10 <sup>4</sup>	(2.5 ± 0.1) × 10 <sup>4</sup>	1.7 ± 0.1	14
	hexane	2.0 ± 0.1	(4.5 ± 0.2) × 10 <sup>3</sup>	(2.9 ± 0.2) × 10 <sup>3</sup>	1.6 ± 0.1	14
<b>B</b> + <b>A</b> (R = CPh <sub>3</sub> )	hexane	0.9 ± 0.1	(1.4 ± 0.1) × 10 <sup>4</sup>	(7.3 ± 0.4) × 10 <sup>3</sup>	1.9 ± 0.2	14
<b>B</b> (R = Ph) + <b>A</b>	hexane	1.6 ± 0.1	(8.6 ± 0.4) × 10 <sup>3</sup>	(5.7 ± 0.3) × 10 <sup>3</sup>	1.5 ± 0.1	14
TEMPO <sup>•</sup> + <b>A</b>	hexane	-0.6 ± 0.1	(7.6 ± 0.4) × 10 <sup>4</sup>	–	–	14
TEMPO <sup>•</sup> + <b>A</b> (R = CPh <sub>3</sub> )	hexane	-1.4 ± 0.1	(1.5 ± 0.1) × 10 <sup>5</sup>	–	–	14
4-oxo-TEMPO <sup>•</sup> + <b>A</b>	hexane	-1.3 ± 0.1	(6.4 ± 0.3) × 10 <sup>4</sup>	–	–	14

<sup>a</sup>  $T = 298$  (this work and ref 18), 300 (ref 13), and 293 K (ref 14); – means not determined. <sup>b</sup> In kcal mol<sup>-1</sup>. <sup>c</sup> Not corrected for the incomplete (98 ± 1%) deuterium enrichment for the TEMPO-H(D) reactions; the true  $k_H/k_D$  values are roughly a factor of 2 higher; see text. <sup>d</sup> Reference 20. <sup>e</sup> This work. <sup>f</sup> PINO<sup>•</sup> = phthalimide *N*-oxyl radical, NHPI = *N*-hydroxyphthalimide. <sup>g</sup> Ar = 2,6-dimethoxyphenyl.

TEMPO-H. The rate constant for D-atom transfer,  $k_{4D,MeCN} = 0.12 \pm 0.02$  M<sup>-1</sup> s<sup>-1</sup> indicates  $k_{4H,MeCN}/k_{4D,MeCN} = 16 \pm 3$  at 298 K. Reaction 4 behaves similarly in CH<sub>2</sub>Cl<sub>2</sub> solvent, showing a similar isotope effect:  $k_{4H,CH_2Cl_2}/k_{4D,CH_2Cl_2} = 13 \pm 2$ .

Rate constants for reactions 2–4 have been measured as a function of temperature over 35–40 K temperature ranges. Selected Eyring plots are shown in Figure 4, and all Eyring and Arrhenius activation parameters are listed in Table 3. Table 4 shows the difference between the H and D activation energies ( $E_{aD} - E_{aH}$ ) and pre-exponential factors,  $\log(A_H/A_D)$ .

**III. Computational Studies.** To investigate the role of tunneling in self-exchange reactions between nitroxyl radicals and hydroxylamines, we performed multidimensional tunneling calculations, using Gaussrate<sup>31</sup> as the interface between Gaussian 03<sup>32</sup> and Polyrate.<sup>33</sup> Our computations were carried out using

both the MPW1K<sup>34</sup> and the more recently developed MO5–2X<sup>35</sup> and MO6<sup>36</sup> functionals. The 6-31+G(d,p) basis set<sup>37</sup> was employed for all of these calculations. Tunneling rates were computed, using the small-curvature tunneling (SCT) approximation.<sup>38</sup>

Because of the computational demands of the tunneling calculations, SCT calculations on the <sup>t</sup>Bu<sub>2</sub>NO<sup>•</sup> + <sup>t</sup>Bu<sub>2</sub>NOH and

(31) Corchado, J. C.; Chuang, Y.-Y.; Coitino, E. L.; Truhlar, D. G. *GAUSSRATE*, version 9.5; University of Minnesota: Minneapolis, MN, 2007.

(32) Frisch, M. J.; et al. *Gaussian 03*, revision D.02; Gaussian, Inc.: Wallingford, CT, 2004.

(33) Corchado, J. C.; et al. *POLYRATE*, version 9.5; University of Minnesota: Minneapolis, MN, 2007.

(34) Lynch, B. J.; Fast, P. L.; Harris, M.; Truhlar, D. G. *J. Phys. Chem. A* **2000**, *104*, 4811.

(35) Zhao, Y.; Schultz, N. E.; Truhlar, D. G. *J. Chem. Theory Comput.* **2006**, *2*, 364–382.

(36) Zhao, Y.; Truhlar, D. G. *Theor. Chem. Acc.* **2008**, *120*, 215–241.

(37) (a) Frisch, M. J.; Pople, J. A.; Binkley, J. S. *J. Chem. Phys.* **1984**, *80*, 3265–3269. (b) Clark, T.; Chandrasekhar, J.; Spitznagel, G. W.; Schleyer, P. v. R. *J. Comput. Chem.* **1983**, *4*, 294–301. (c) Hehre, W. J.; Ditchfield, R.; Pople, J. A. *J. Chem. Phys.* **1972**, *56*, 2257–2261.

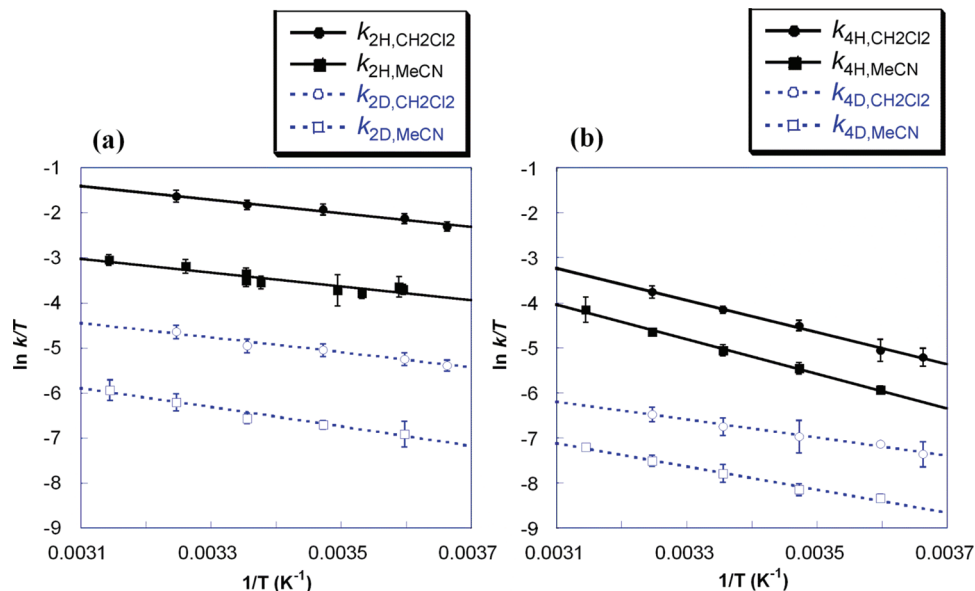


**Figure 4.** Eyring plots for (a) 4-oxo-TEMPO\* + TEMPO-H (reaction 2) and (b) tBu<sub>2</sub>NO\* + TEMPO-H (reaction 4), both in MeCN and CH<sub>2</sub>Cl<sub>2</sub>.

**Table 3.** Eyring and Arrhenius Parameters for H- and D-Atom Transfer Reactions<sup>a</sup>

reaction	solvent	T (K)	ΔH <sup>‡</sup>	ΔS <sup>‡</sup>	E <sub>a</sub>	log A
4-oxo-TEMPO* + TEMPO-H <sup>b</sup>	MeCN	278–318	3.0 ± 0.5	−43 ± 3	3.6 ± 0.5	3.8 ± 0.6
4-oxo-TEMPO* + TEMPO-D	MeCN	278–318	4.3 ± 0.4	−46 ± 2	4.9 ± 0.4	3.3 ± 0.4
4-oxo-TEMPO* + TEMPO-H	CH <sub>2</sub> Cl <sub>2</sub>	273–308	3.0 ± 0.4	−41 ± 2	3.6 ± 0.4	4.3 ± 0.4
4-oxo-TEMPO* + TEMPO-D	CH <sub>2</sub> Cl <sub>2</sub>	273–308	3.3 ± 0.4	−46 ± 2	3.9 ± 0.4	3.2 ± 0.4
4-oxo-TEMPO* + 4-MeO-TEMPO-H	MeCN	278–318	4.8 ± 0.3	−38 ± 2	5.4 ± 0.3	4.9 ± 0.4
4-oxo-TEMPO* + 4-MeO-TEMPO-D	MeCN	288–328	5.4 ± 0.3	−42 ± 2	6.0 ± 0.3	4.0 ± 0.4
tBu <sub>2</sub> NO* + TEMPO-H	MeCN	278–318	7.7 ± 0.3	−31 ± 2	8.3 ± 0.3	6.4 ± 0.4
tBu <sub>2</sub> NO* + TEMPO-D	MeCN	278–318	5.1 ± 0.3	−45 ± 2	5.7 ± 0.3	3.3 ± 0.4
tBu <sub>2</sub> NO* + TEMPO-H	CH <sub>2</sub> Cl <sub>2</sub>	273–308	7.1 ± 0.3	−32 ± 2	7.6 ± 0.3	6.3 ± 0.4
tBu <sub>2</sub> NO* + TEMPO-D	CH <sub>2</sub> Cl <sub>2</sub>	273–308	4.0 ± 0.3	−47 ± 2	4.5 ± 0.3	2.9 ± 0.4
PINO* + 4Me-NHPI <sup>c</sup>	AcOH	290–309	9.8 ± 0.2	−13 ± 1	10.4 ± 0.2	10.4 ± 0.2
4-Me-PINO* + NHPI <sup>c</sup>	AcOH	290–309	10.0 ± 0.2	−13 ± 1	10.6 ± 0.2	10.4 ± 0.2

<sup>a</sup> ΔH<sup>‡</sup>, E<sub>a</sub> in kcal mol<sup>−1</sup>; ΔS<sup>‡</sup> in cal mol<sup>−1</sup> K<sup>−1</sup>. <sup>b</sup> Originally reported in ref 20. <sup>c</sup> Reference 18.

**Table 4.** Kinetic Isotope Effects and Differences in Protio and Deutero Arrhenius Parameters<sup>a</sup>

reaction	solvent	k <sub>H</sub> /k <sub>D</sub>	E <sub>aD</sub> − E <sub>aH</sub>	log(A <sub>H</sub> /A <sub>D</sub> )
4-oxo-TEMPO* + TEMPO-H	MeCN	23 ± 3	1.3 ± 0.6	0.5 ± 0.7
4-oxo-TEMPO* + TEMPO-H	CH <sub>2</sub> Cl <sub>2</sub>	23 ± 4	0.3 ± 0.6	1.1 ± 0.6
4-oxo-TEMPO* + 4-MeO-TEMPO-H	MeCN	21 ± 3	0.6 ± 0.4	0.9 ± 0.6
tBu <sub>2</sub> NO* + TEMPO-H	MeCN	16 ± 3	−2.6 ± 0.4	3.1 ± 0.6
tBu <sub>2</sub> NO* + TEMPO-H	CH <sub>2</sub> Cl <sub>2</sub>	13 ± 2	−3.1 ± 0.4	3.4 ± 0.6

<sup>a</sup> k<sub>H</sub>/k<sub>D</sub> at 298 K, E<sub>aD</sub> − E<sub>aH</sub> in kcal mol<sup>−1</sup>.

**Table 5.** Computed Canonical Variational Transition State Theory (CVT) and Small Curvature Tunneling (SCT) Rate Constants and Arrhenius Activation Parameters for at the MPW1K/6-31+G(d,p) Level of Theory<sup>a</sup>

reaction	method	k <sub>H</sub>	k <sub>D</sub>	k <sub>H</sub> /k <sub>D</sub>	E <sub>a,H</sub>	log(A <sub>H</sub> )	E <sub>a,D</sub>	log(A <sub>D</sub> )
Me <sub>2</sub> NO* + HONMe <sub>2</sub>	CVT	5.65 × 10 <sup>−4</sup>	8.67 × 10 <sup>−5</sup>	6.5	14.8	7.6	15.8	7.6
Me <sub>2</sub> NO* + HONMe <sub>2</sub>	SCT	4.85 × 10 <sup>1</sup>	2.47 × 10 <sup>−1</sup>	196	6.1	6.2	7.3	4.8
MeHNO* + HONHMe	SCT	1.83 × 10 <sup>1</sup>	7.65 × 10 <sup>−2</sup>	239	6.1	5.8	7.4	4.3

<sup>a</sup> k<sub>H</sub>, k<sub>D</sub>, M<sup>−1</sup> s<sup>−1</sup>; E<sub>a,H</sub>, E<sub>a,D</sub>, kcal mol<sup>−1</sup>.

TEMPO\* + TEMPO-H systems were too big to be practical. Therefore, we began by performing calculations on (CH<sub>3</sub>)<sub>2</sub>NO\* + (CH<sub>3</sub>)<sub>2</sub>NOH. The calculated rate constants, activation parameters, and H/D kinetic isotope effects for this reaction are given in Table 5.

(38) Fernandez-Ramos, A.; Ellingson, B. A.; Garrett, B. C.; Truhlar, D. G. In *Reviews in Computational Chemistry*, Vol. 23; Lipkowitz K. B., Cundari, T. R., Eds.; Wiley-VCH: Hoboken, NJ, 2007; pp 125–232.

The transition structure (TS) for (CH<sub>3</sub>)<sub>2</sub>NO\* + (CH<sub>3</sub>)<sub>2</sub>NOH, shown in Figure 5a, has C<sub>2h</sub> symmetry. The SCT calculations start at this TS and descend down a minimum energy path toward the reactants/products. Unfortunately, starting from the TS and moving along this reaction coordinate, the C<sub>s</sub> plane of symmetry was maintained throughout the reaction. Consequently, the SCT calculations did not lead to the hydrogen-bonded reactant complex (CH<sub>3</sub>)<sub>2</sub>NOH⋯ON(CH<sub>3</sub>)<sub>2</sub>, which has C<sub>1</sub> symmetry (Figure 5b). Instead, the calculations led to the

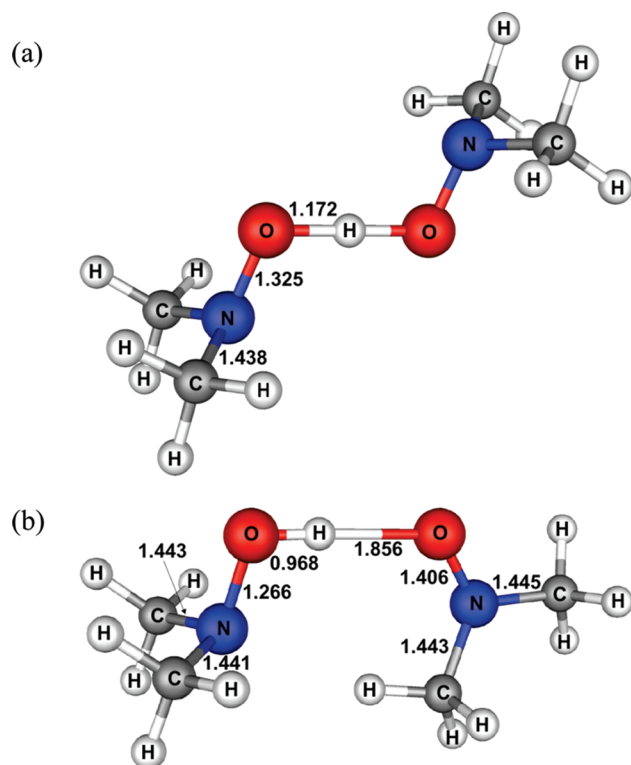


**Figure 5.** (a) Transition structure for hydrogen transfer between  $(\text{CH}_3)_2\text{NOH}$  and  $(\text{CH}_3)_2\text{NO}^*$ . (b) H-bonded complex between  $(\text{CH}_3)_2\text{NOH}$  and  $(\text{CH}_3)_2\text{NO}^*$ . Bond lengths are in Ångstroms.

$C_s$  TS that connects the two enantiomeric geometries of the reactant complex. Destroying the  $C_s$  plane in the  $C_{2h}$  TS by substituting two  $\text{CD}_3$  for two  $\text{CH}_3$  groups failed to coax the hydrogen-bonded complex to depart from the ridge on the potential energy surface that connects the two enantiomers.

However, we were able to follow the reaction path back from the TS to the reactants for the self-exchange reaction between the monomethylnitroxyl radical and the monomethyl-hydroxylamine. The calculated values of  $k_H$ ,  $E_a$ ,  $A$ , and  $k_H/k_D$  for this reaction,  $(\text{CH}_3)\text{HNO}^* + \text{HONH}(\text{CH}_3)$ , are also given in Table 5. The SCT results for the two reactions are close enough to lead us to believe that the computational results for the dimethyl reaction are reliable, despite our being unable to follow the reaction path all the way back to the reactant complex in this case. Most of the tunneling seems to originate from regions along the reaction path that are closer to the TS, where the reaction barrier is narrow, than from regions close to the reactants, where the barrier is much wider and the deviation from  $C_s$  symmetry is significant.

The formation of the  $(\text{CH}_3)_2\text{NOH}\cdots\text{ON}(\text{CH}_3)_2$  reactant complex (Figure 5B) from the separated reactants is enthalpically favorable:  $\Delta H = -4.6 \text{ kcal mol}^{-1}$  [calculated with MPW1K/6-31+G(d,p)]. However, the entropy of complex formation [ $\Delta S = -26.7 \text{ cal K}^{-1} \text{ mol}^{-1}$ ] is so unfavorable that the calculated value of the gas phase equilibrium constant [ $K = 1.4 \times 10^{-4} \text{ M}^{-1}$ ] at 298 K is small. Since at 298 K the reactants are lower in free energy than the reactant complex, the computed rate constants,  $A$  factors, and activation energies reported in Table 5 are for reactions starting from the separated reactants.

We used all three functionals—MPW1K, MO5-2X, and MO6—to calculate the barrier height for the hydrogen self-exchange reaction,  $(\text{CH}_3)_2\text{NO}^* + (\text{CH}_3)_2\text{NOH}$ , starting from the

$C_1$  reactant complex. All three functionals gave enthalpies of activation for passage over the reaction barrier that were the same to within  $1.0 \text{ kcal mol}^{-1}$ . Therefore, we elected to do the tunneling calculations with just one of them, MPW1K.

The MPW1K rate constants at 298 K for the hydrogen and deuterium self-exchange reactions were computed by canonical variational transition state theory (CVT) for passage over the barrier and by small curvature tunneling (SCT) calculations for passage through the barrier. The results are contained in Table 5. The Arrhenius activation parameters, obtained from the temperature dependences of the calculated rate constants around 298 K, are also given in Table 5.

The  $k_H$  values in Table 5 show that the SCT rate constant for hydrogen tunneling through the barrier is computed to be larger than the CVT rate constant for passage over it by a factor of about  $10^5$ . Tunneling reduces  $E_a$  by  $8.7 \text{ kcal mol}^{-1}$  for hydrogen, with a decrease in  $\log A$  of only 1.4. The large reduction in  $E_a$  and the small decrease in  $\log A$  shows that our SCT calculations predict that tunneling is very efficient in  $(\text{CH}_3)_2\text{NO}^* + (\text{CH}_3)_2\text{NOH}$ . The width of the barrier to this reaction is computed to be only  $0.42 \text{ \AA}$ , which is presumably why tunneling is computed to be so effective at increasing the reaction rate.

Table 5 also contains the results of our calculations for deuterium self-exchange in  $(\text{CH}_3)_2\text{NO}^* + (\text{CH}_3)_2\text{NOD}$ . Comparison of the CVT and SCT rate constants for D shows that tunneling is also predicted to dominate the reaction involving deuterium. However, a very large H/D KIE of  $k_H/k_D = 196$  is predicted for tunneling. Of this ratio, a factor of 7.4 is due to H tunneling with a  $1.2 \text{ kcal mol}^{-1}$  lower  $E_a$  than D. An even larger factor is due to  $\log A_H$  being about 1.4 larger than  $\log A_D$ . Even though H is calculated to tunnel through the barrier at an average energy of about  $1.2 \text{ kcal mol}^{-1}$  lower than D, H is calculated to tunnel with a higher probability than D by a factor of 26.5.<sup>39</sup>

Our SCT value of H/D KIE of 196 for  $(\text{CH}_3)_2\text{NO}^* + (\text{CH}_3)_2\text{NOH/D}$  is about a factor of 9 larger than the apparent experimental values for reaction of TEMPO-H with a variety of nitroxide radicals (Table 2). However, as already noted, the true H/D KIEs are substantially larger than the values given in Table 2, because of the incomplete D enrichment. For TEMPO-H/D + 4-oxo-TEMPO\*, the measured  $k_H/k_D$  of  $23$  at  $98 \pm 1\%$  D corresponds to a true KIE of about 40 (the  $98 \pm 1\%$  range gives values of 30–70).

The calculated bimolecular SCT rate constant of  $k = 48.5 \text{ M}^{-1} \text{ s}^{-1}$  is in excellent agreement with the rate constants in Table 2 for the TEMPO-H reactions. The closest experimental analogy to this gas phase rate constant is the  $k$  of  $300 \text{ M}^{-1} \text{ s}^{-1}$  for 4-oxo-TEMPO\* + TEMPO-H in  $\text{CCl}_4$ , which has  $\Delta G^\circ \approx -1 \text{ kcal mol}^{-1}$ . In contrast, the CVT rate constant of  $k = 5.65 \times 10^{-4} \text{ M}^{-1} \text{ s}^{-1}$  for  $(\text{CH}_3)_2\text{NO}^* + (\text{CH}_3)_2\text{NOH}$  underestimates the experimental rate constants (Table 2) by a factor of  $10^4$ – $10^6$ . Thus, our calculations on both the rate of and H/D KIE for this model reaction strongly support the conclusion that the dialkyl-nitroxyl radical reactions in Table 2 all occur by tunneling through the reaction barrier, rather than by passage over it.

Although we were unable to perform SCT calculations on larger systems, we did carry out CVT calculations on the

(39) When the tunneling distance is large, there is a temperature range in which D tunnels considerably closer to the top of the barrier than H, so that the probability of passing through or over the barrier is actually greater for D than for H. As a result, in this temperature range,  $E_{a,D} - E_{a,H} > 1.3 \text{ kcal/mol}$ , but  $\log(A_H/A_D) < 0$ . See, for example, Shelton, G. R.; Hrovat, D. A.; Borden, W. T. *J. Am. Chem. Soc.* **2007**, *129*, 164.



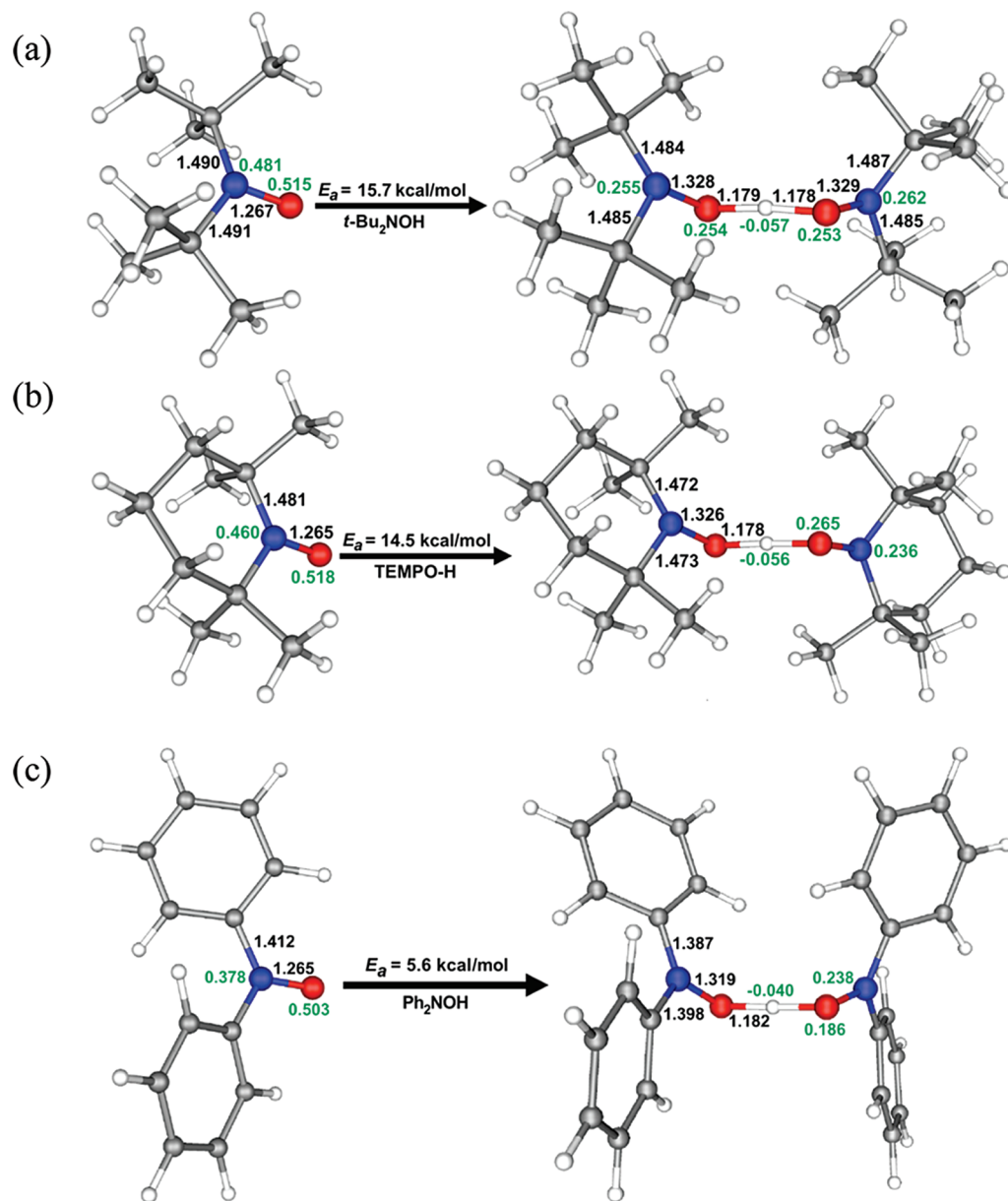


**Figure 6.** Bond lengths (Å), atomic spin densities (in green), and activation energies (kcal mol<sup>-1</sup>) for the nitroxyl radicals, (a)  $t\text{-Bu}_2\text{NO}^*$ , (b)  $\text{TEMPO}^*$ , and (c)  $\text{Ph}_2\text{NO}^*$ , and the transition structures and CVT activation energies for their hydrogen self-exchange reactions with the corresponding hydroxylamines.

$t\text{-Bu}_2\text{NO}^*(\text{H})$ ,  $\text{TEMPO}^*(\text{H})$  and  $\text{Ph}_2\text{NO}^*(\text{H})$  self-exchange reactions. For each one, the TS was located and confirmed to have one imaginary frequency by a vibrational analysis. Key features of the geometries of the nitroxide reactants and the self-exchange TSs are given in Figure 6, along with the calculated  $E_a$  values from CVT for each reaction.

As shown in Figure 6, the geometries of the TSs for all three reactions are very similar. In each TS the O–H bonds

approximately bisect the C–N–C angles, strongly suggesting that the electron and the proton are transferred together between the same AO on each oxygen. This inference is confirmed by inspection of the SOMOs for the three TSs, which are shown in Figure 7. Thus, all three reactions proceed by a mechanism in which a hydrogen atom is transferred between a pair of oxygen AOs, rather than by a mechanism in which a proton is transferred between one pair of oxygen AOs and an electron is transferred between a different pair of oxygen AOs (which in some contexts has been called proton-coupled electron transfer, PCET).<sup>40</sup>

The CVT activation energies for the dialkylnitroxyl reactions,  $E_a = 15.7$  and  $14.5$  kcal mol<sup>-1</sup> for  $t\text{-Bu}_2\text{NO}^* + t\text{-Bu}_2\text{NOH}$  and  $\text{TEMPO}^* + \text{TEMPO-H}$ , respectively, are much larger than the corresponding energy for  $\text{Ph}_2\text{NO}^* + \text{Ph}_2\text{NOH}$ ,  $E_a = 5.6$  kcal mol<sup>-1</sup>. This is in pleasing agreement with the experimental finding that the rate constant for  $\text{Ph}_2\text{NO}^* + \text{Ph}_2\text{NOH}$ <sup>13</sup> is at least

(40) In some circumstances, it is valuable to distinguish between an “HAT mechanism,” where the  $e^-$  and  $\text{H}^+$  come from the same AO, and transfer to the same AO, vs a “PCET mechanism,” in which the two particles are transferred between different sets of AOs in the transition structure. (a) Mayer, J. M.; Hrovat, D. A.; Thomas, J. L.; Borden, W. T. *J. Am. Chem. Soc.* **2002**, *124*, 11142–11147. (b) Litwinienko, G.; Ingold, K. U. *Acc. Chem. Res.* **2007**, *40*, 222–230. See the discussion in: (c) Waidmann, C. R.; Zhou, X.; Tsai, E. A.; Kaminsky, W.; Hrovat, D. A.; Borden, W. T.; Mayer, J. M. *J. Am. Chem. Soc.* **2009**, *131*, 4729–4743.



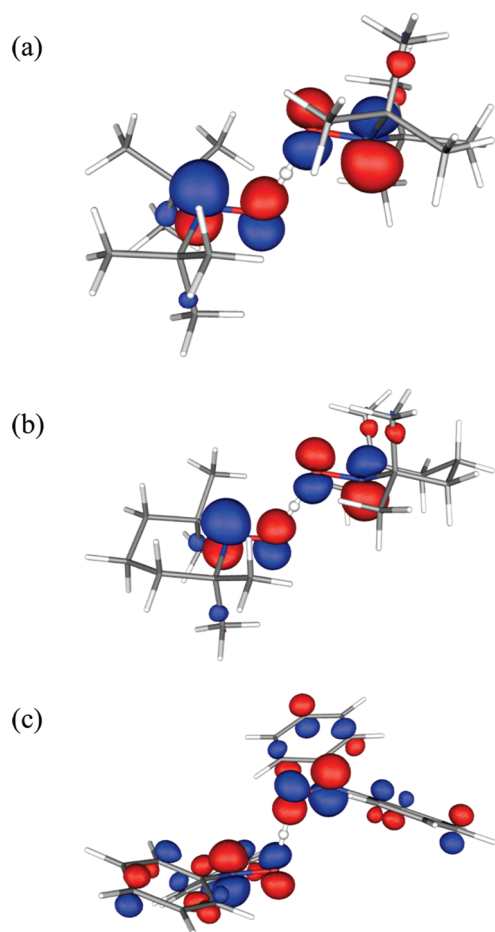


**Figure 7.** SOMOs of the transition structures for hydrogen exchange reactions: (a)  ${}^{\bullet}\text{Bu}_2\text{NO} + {}^{\bullet}\text{Bu}_2\text{NOH}$ , (b)  $\text{TEMPO}^{\bullet} + \text{TEMPO-H}$ , and (c)  $\text{Ph}_2\text{NO}^{\bullet} + \text{Ph}_2\text{NOH}$ .

5 orders of magnitude faster than those for  ${}^{\bullet}\text{Bu}_2\text{NO} + {}^{\bullet}\text{Bu}_2\text{NOH}$ <sup>13</sup> and  $\text{TEMPO}^{\bullet} + \text{TEMPO-H}$ . Comparisons of the geometries and spin densities of the nitroxide reactants and TSs in Figure 6 indicates that the phenyl groups lower the barrier to reaction by providing greater delocalization of the unpaired electron in the TS for  $\text{Ph}_2\text{NO}^{\bullet} + \text{Ph}_2\text{NOH}$  reaction than in the  $\text{Ph}_2\text{NO}^{\bullet}$  reactant.

In the nitroxyl radicals, the unpaired spin density of 0.88 in the N–O group of  $\text{Ph}_2\text{NO}^{\bullet}$  is about 0.1 smaller than the unpaired spin densities of 0.98 and 1.00 in the NO groups of  $\text{TEMPO}^{\bullet}$  and  ${}^{\bullet}\text{Bu}_2\text{NO}^{\bullet}$ , respectively. The C–N bond lengths in  $\text{Ph}_2\text{NO}^{\bullet}$  are calculated to be 0.07 and 0.08 Å shorter than those in  $\text{TEMPO}^{\bullet}$  and  ${}^{\bullet}\text{Bu}_2\text{NO}^{\bullet}$ , respectively. This is a larger difference than the  $\sim 0.04$  Å difference in covalent radii between  $\text{sp}^2$  and  $\text{sp}^3$  carbon atoms. These results indicate that the phenyl groups in  $\text{Ph}_2\text{NO}^{\bullet}$  delocalize the unpaired electron in the two-center, three-electron N–O  $\pi$  bond.

On going from the reactants to the TS, the four C–N bond lengths in  $\text{Ph}_2\text{NO}^{\bullet}$  shorten by an average of 0.02 Å; whereas the C–N bond lengths in  $\text{TEMPO}^{\bullet}$  and  ${}^{\bullet}\text{Bu}_2\text{NO}^{\bullet}$  shorten by less than 0.01 Å. In addition, the spin densities in the NO groups of the  $\text{Ph}_2\text{NO}^{\bullet} + \text{Ph}_2\text{NOH}$  TS are 0.08 smaller than the spin density in the NO group of  $\text{Ph}_2\text{NO}^{\bullet}$ ; whereas, the corresponding decrease in the spin densities in the NO groups is only about 0.03 in both  $\text{TEMPO}^{\bullet} + \text{TEMPO-H}$  and  ${}^{\bullet}\text{Bu}_2\text{NO}^{\bullet} + {}^{\bullet}\text{Bu}_2\text{NOH}$ . The larger decreases in the C–N bond lengths and in the NO spin densities between the  $\text{Ph}_2\text{NO}^{\bullet}$  reactants and the TS for  $\text{Ph}_2\text{NO}^{\bullet}$

+  $\text{Ph}_2\text{NOH}$  are both consistent with the TS for this reaction being stabilized by electron delocalization into the phenyl groups. We believe that this is the reason why the hydrogen self-exchange reaction of this diarylnitroxyl radical is many orders of magnitude faster than those of the dialkylnitroxyl radicals in Table 2.

## Discussion

Nitroxyl radical plus hydroxylamine reactions have been studied experimentally and computationally. The experimental reactions (eqs 2–4) are close to isoergic in both MeCN and  $\text{CH}_2\text{Cl}_2$ , with  $|\Delta G^{\circ}| \leq 1.4$  kcal mol<sup>-1</sup> (Table 2), and involve reagents that are sterically quite similar. Thus these reactions are good approximations of self-exchange reactions. Self-exchange reactions are inherently simpler to analyze than non-degenerate reactions. The symmetry of self-exchange reactions requires that the transition structure, or, more generally, the seam on the potential energy surface, be symmetrically placed between the reactant and product.

Thermochemical data show that the reactions in eqs 2–4 must occur by concerted rather than stepwise transfer of the proton and electron. For self-exchange reactions, the potential stepwise mechanisms with initial electron or proton transfer are the microscopic reverse of each other.<sup>41</sup> For the  $\text{TEMPO}^{\bullet} + \text{TEMPO-H}$  self-exchange reaction, both possible stepwise pathways proceed through a  $\text{TEMPO}^- + \text{TEMPO-H}^+$  intermediate state. Based on the known  $E_{1/2}$  and  $\text{p}K_a$  values, this state is about 60 kcal mol<sup>-1</sup> higher than  $\text{TEMPO}^{\bullet} + \text{TEMPO-H}$  (2.6 V or 44  $\text{p}K_a$  units).<sup>42</sup> For the pseudo self-exchange reactions in eqs 2–4, the data are not available to make a full analysis, but the  $E_{1/2}$  and  $\text{p}K_a$  values are not very different for the various compounds,<sup>26</sup> so these reactions will also have potential intermediate states lying *ca.* 60 kcal mol<sup>-1</sup> uphill. This is dramatically higher than the Eyring barriers  $\Delta G^{\ddagger} < 20$  kcal mol<sup>-1</sup> found for reactions 2–4. Thus the stepwise pathways are not possible, and the reaction must occur by concerted  $\text{H}^+/\text{e}^-$  transfer.

**I. Solvent Effects.** The experimental rate constants are faster in less polar and less hydrogen-bonding solvents (Table 2). For 4-oxo- $\text{TEMPO}^{\bullet} + \text{TEMPO-H}$ , the rate constants are 10, 48, and 300 M<sup>-1</sup> s<sup>-1</sup> in MeCN,  $\text{CH}_2\text{Cl}_2$ , and  $\text{CCl}_4$ , respectively. Litwinienko, Ingold, et al. have shown that for HAT reactions of phenols, solvent effects on the rate constants are predominantly due to the formation of a hydrogen bond between the H-atom donor and the solvent.<sup>43</sup> Only the fraction of the phenol that is not hydrogen bonded is reactive, and the reactivity of the non-hydrogen bonded phenol is not significantly affected by solvent. Qualitatively, this explains why the  $\text{TEMPO-H}$

(41) Roth, J. P.; Lovell, S.; Mayer, J. M. *J. Am. Chem. Soc.* **2000**, *122*, 5486.

(42) (a)  $\Delta G^{\circ}(\text{ET}) = -23.1[E(\text{TEMPO}^{\bullet}) - E(\text{TEMPO-H})] \approx 60$  kcal mol<sup>-1</sup>  $\Delta G^{\circ}(\text{PT}) = -1.37[\text{p}K_a(\text{TEMPO-H}^+) - \text{p}K_a(\text{TEMPO-H})] = \Delta G^{\circ}(\text{ET})$ . (b)  $E(\text{TEMPO}^{\bullet}) \approx -1.91$  V versus  $\text{Cp}_2\text{Fe}^{+/0}$ ; Mori, Y.; Sakaguchi, Y.; Hayashi, H. *J. Phys. Chem. A* **2000**, *104*, 4896. (c)  $E(\text{TEMPO-H}) \approx 0.71$  V versus  $\text{Cp}_2\text{Fe}^{+/0}$ ; Semmelhack, M. F.; Chou, C. S.; Cortes, D. A. *J. Am. Chem. Soc.* **1983**, *105*, 4492–4494. (d)  $\text{p}K_a(\text{TEMPO-H}) \approx 41$  in MeCN is estimated from  $\text{p}K_a(\text{TEMPO-H}) = 31.0$  in DMSO.<sup>26</sup> (e)  $\text{p}K_a$  conversion from DMSO to MeCN: Chantooni, M. K., Jr.; Kolthoff, I. M. *J. Phys. Chem.* **1976**, *80*, 1306–1310. (f)  $\text{p}K_a(\text{TEMPO-H}^+) = \text{p}K_a(\text{TEMPO-H}) + 23.1[E(\text{TEMPO}^{\bullet}) - E(\text{TEMPO-H})]/1.37 \approx -3$ .

(43) (a) Avila, D. V.; Ingold, K. U.; Luszyk, J.; Green, W. H.; Procopio, D. R. *J. Am. Chem. Soc.* **1995**, *117*, 2929–30. (b) Valgimigli, L.; Banks, J. T.; Ingold, K. U.; Luszyk, J. *J. Am. Chem. Soc.* **1995**, *117*, 9966–71. (c) Snelgrove, D. W.; Luszyk, J.; Banks, J. T.; Mulder, P.; Ingold, K. U. *J. Am. Chem. Soc.* **2001**, *123*, 469–477.

reactions are slower in MeCN, a good hydrogen bond acceptor, than in chlorinated solvents. The formation of TEMPO-H $\cdots$ NCMe hydrogen bonds is indicated by the TEMPO-H O–H stretching frequency in CD<sub>3</sub>CN (3495 cm<sup>-1</sup>), being  $\sim$ 100 cm<sup>-1</sup> lower than  $\nu$ (TEMPO-H) in CD<sub>2</sub>Cl<sub>2</sub> (3583 cm<sup>-1</sup>) and CCl<sub>4</sub> (3597 cm<sup>-1</sup>). A recent crystal structure of TEMPO-H shows hydrogen bonds between TEMPO-H molecules with O $\cdots$ O distances of 2.83 and 2.88 Å.<sup>23</sup>

Quantitatively, the Litwinienko and Ingold model predicts that the solvent effect will be independent of the H-atom acceptor.<sup>44,45</sup> However, the experimental ratios of rate constants in CH<sub>2</sub>Cl<sub>2</sub> vs MeCN are  $4.8 \pm 0.6$  for 4-oxo-TEMPO $\cdot$  + TEMPO-H and  $2.4 \pm 0.3$  for 'Bu<sub>2</sub>NO $\cdot$ ' + TEMPO-H.<sup>44</sup> The 4-oxo-TEMPO $\cdot$  + TEMPO-H reaction (eq 2) appears to be affected by solvent polarity as well as hydrogen bonding, as it is 6 times faster in CCl<sub>4</sub> than in CH<sub>2</sub>Cl<sub>2</sub> (Table 2). A more dramatic effect has been reported for the 'BuArNO $\cdot$ '/'BuArNOH self-exchange reaction (Ar = 2,6-dimethoxyphenyl), which is more than a hundred times faster in CCl<sub>4</sub> than in CHCl<sub>3</sub> and CH<sub>2</sub>Cl<sub>2</sub>:  $2 \times 10^3$  versus  $<20 \text{ M}^{-1} \text{ s}^{-1}$ .<sup>13</sup> A reviewer has suggested that these anomalous kinetic solvent effects may be due to changes in the nitroxyl radical spin density with solvent,<sup>46</sup> which are known to affect their rate constant for reaction with alkyl radicals.<sup>47</sup>

## II. Kinetic Isotope Effects and Evidence for Tunneling.

Hydrogen tunneling is suggested by the large  $k_{\text{H}}/k_{\text{D}}$  values of  $23 \pm 3$ ,  $21 \pm 3$ , and  $16 \pm 3$  at 298 K for reactions 2–4 in MeCN. A one-dimensional semiclassical transition state theory model, taking  $\Delta G_{\text{D}}^{\ddagger} - \Delta G_{\text{H}}^{\ddagger}$  to be at most the difference in zero-point energies, predicts a maximum  $k_{\text{H}}/k_{\text{D}}$  of 9 at 298 K using the measured OH and OD stretches.<sup>3,4,48</sup> A more complete semiclassical model including bending modes gives a maximum KIE of about 13 for cleavage of an O–H bond.<sup>3</sup> The computed CVT H/D KIEs at 298 K, without tunneling, are 6.5, 4.9, 4.9, and 4.7 for the self-exchange reactions involving Me<sub>2</sub>NO $\cdot$ ,

'Bu<sub>2</sub>NO $\cdot$ ', TEMPO $\cdot$ , and Ph<sub>2</sub>NO $\cdot$ . These computed H/D KIEs are all significantly lower than the measured values for reactions 2–4, but they are *ca.* three times larger than the KIEs in Table 2 for reactions involving monoarylhydroxylamines, including the 'Bu(Ar)NO $\cdot$ ' + 'Bu(Ar)NOH self-exchange [Ar = 2,6-(MeO)<sub>2</sub>C<sub>6</sub>H<sub>3</sub>].

The experimental activation energies also provide evidence for tunneling. According to Bell,<sup>3</sup> tunneling is indicated when  $E_{\text{aD}} - E_{\text{aH}}$  is larger than the difference in zero-point energies, 1.3 kcal mol<sup>-1</sup> in this case,<sup>48</sup> and/or when there are significant differences in the pre-exponential terms,  $A_{\text{H}}/A_{\text{D}} < 0.7$  or  $A_{\text{H}}/A_{\text{D}} > 1.4$ , or  $|\log(A_{\text{H}}/A_{\text{D}})| > 0.15$ . All of the reactions studied here have  $\log(A_{\text{H}}/A_{\text{D}})$  larger than this semiclassical limit, except perhaps for reaction 2 in MeCN which has  $\log(A_{\text{H}}/A_{\text{D}}) = 0.5 \pm 0.7$  (Table 4). For reactions 2 and 3, the positive values of  $\log(A_{\text{H}}/A_{\text{D}})$ , the low values of both  $A_{\text{H}}$  and  $A_{\text{D}}$  ( $<10^5 \text{ M}^{-1} \text{ s}^{-1}$ ), and low  $E_{\text{a}}$  ( $<6 \text{ kcal mol}^{-1}$ ) values all suggest that there is significant tunneling in the reactions of both the H and D isotopomers.<sup>5</sup>

The small-curvature tunneling calculations on (CH<sub>3</sub>)<sub>2</sub>NO $\cdot$  + (CH<sub>3</sub>)<sub>2</sub>NOH also show that tunneling is the dominant pathway in this model reaction for a self-exchange involving a dialkyl-nitroxyl radical reacting with a dialkylhydroxylamine. Tunneling through the barrier is computed to be about 10<sup>5</sup> times faster than passage over the barrier for H, and more than 10<sup>3</sup> times faster, even for D. The experimental KIEs vary little with solvent, indicating that the solvent plays little role in the tunneling process.<sup>49</sup>

The 'Bu<sub>2</sub>NO $\cdot$ ' + TEMPO-H reaction (eq 4) is found to have very unusual activation parameters. These data derive from quite small changes in absorbance (see above), but they are based on three separate measurements of rate constants at each temperature, with consistent multiple stopped-flow runs in each measurement. The resulting  $A_{\text{H}}$  is a thousand times larger than  $A_{\text{D}}$  both in MeCN and CH<sub>2</sub>Cl<sub>2</sub>, and  $E_{\text{aD}}$  is substantially smaller than  $E_{\text{aH}}$ :  $E_{\text{aD}} - E_{\text{aH}} = -2.5 \pm 0.4$  in MeCN and  $-3.1 \pm 0.4 \text{ kcal mol}^{-1}$  in CH<sub>2</sub>Cl<sub>2</sub>. That  $E_{\text{aD}} < E_{\text{aH}}$  is indicated by the increase in  $k_{\text{H}}/k_{\text{D}}$  values with temperature, in MeCN from  $11 \pm 1$  at 278 K to  $17 \pm 2$  at 308 K and  $21 \pm 6$  at 318 K. These values are surprising both because they are so different than those for the very similar reactions 2 and 3,<sup>50</sup> and because  $E_{\text{aD}} < E_{\text{aH}}$  is opposite to the predictions of both semiclassical and tunneling models.<sup>3,5</sup> While similar unusual activation parameters have been reported for two other HAT/PCET reactions,<sup>51</sup> we are not sure of the origin in this case. It is interesting that the formation of the hydrogen-bonded precursor complex in this reaction, TEMPO-H/D $\cdots$ ON'Bu<sub>2</sub>, also appears to be isotopically sensitive (see above).<sup>17,52</sup>

In light of the importance of tunneling for the TEMPO $\cdot$ /TEMPO-H self-exchange reaction, the success of the Marcus cross relation for reactions involving TEMPO $\cdot$  is perhaps surprising. The cross relation is a semiclassical treatment that

- (44) (a) In the Litwinienko/Ingold/Abraham model,<sup>43,44b,c</sup> the CH<sub>2</sub>Cl<sub>2</sub>/MeCN kinetic solvent effect is given by  $\log(k_{\text{CH}_2\text{Cl}_2}/k_{\text{MeCN}}) = 8.3\alpha_2^{\text{H}}(\beta_2^{\text{H}}_{\text{MeCN}} - \beta_2^{\text{H}}_{\text{CH}_2\text{Cl}_2})$ . Using  $\alpha_2^{\text{H}}$  (the solute constant) = 0.29 for dialkylhydroxylamines and  $\beta_2^{\text{H}}$  (the hydrogen-bond acceptor solvent constant) = 0.44 for MeCN and 0.05 for CH<sub>2</sub>Cl<sub>2</sub>,<sup>45</sup> this model predicts  $k_{\text{CH}_2\text{Cl}_2}/k_{\text{MeCN}} = 8.7$ , in modest agreement with the experimental values of  $4.8 \pm 0.6$  and  $2.4 \pm 0.3$  for reactions 2 and 4. However, in our experience<sup>44d</sup> this model is not very accurate for reactions in CH<sub>2</sub>Cl<sub>2</sub> (see ref 45). The Ingold/Abraham model may be incomplete for this example because the interaction of TEMPO ( $\beta_2^{\text{H}} = 0.46$ ) with CH<sub>2</sub>Cl<sub>2</sub> ( $\alpha_2^{\text{H}} = 0.15$ ) may be as important as the interaction of TEMPOH with CH<sub>2</sub>Cl<sub>2</sub>. The radical-solvent interaction is absent in many radical reactions because  $\alpha_2^{\text{H}}$  (solvent) or  $\beta_2^{\text{H}}$ (RO $\cdot$ ) is negligible. (b) Abraham, M. H.; Grellier, P. L.; Prior, D. V.; Morris, J. J.; Taylor, P. J. *J. Chem. Soc., Perkin Trans. 2* **1990**, 521. (c) Abraham, M. H.; Grellier, P. L.; Prior, D. V.; Duce, P. P.; Morris, J. J.; Taylor, P. J. *J. Chem. Soc., Perkin Trans. 2* **1989**, 699. (d) Warren, J. J., unpublished results.
- (45) (a) The  $\beta_2^{\text{H}}$  is given as 0.05 for CH<sub>2</sub>Cl<sub>2</sub> by Abraham et al.<sup>44b,44c</sup> A different value of 0.15 has been suggested using the KSE model,<sup>45b</sup> which was later revised to 0.20.<sup>45c</sup> As pointed out by a reviewer, the agreement with the KSE model is better using these revised values. However, we feel that the KSE model becomes less compelling when the  $\beta_2^{\text{H}}$  values are not independent parameters but rather extracted from the radical reaction rates. (b) Galian, R. E.; Litwinienko, G.; Pérez-Prieto, J.; Ingold, K. U. *J. Am. Chem. Soc.* **2007**, *129*, 9280–9281. (c) Foti, M. C.; Daquino, C.; Mackie, I. D.; DiLabio, G. A.; Ingold, K. U. *J. Org. Chem.* **2008**, *73*, 9270–9282.
- (46) (a) Knauer, B. R.; Napier, J. J. *J. Am. Chem. Soc.* **1976**, *98*, 4395–4400. (b) Improta, R.; Barone, V. *Chem. Rev.* **2004**, *104*, 1231–1254.
- (47) Beckwith, A. L. J.; Bowry, V. W.; Ingold, K. U. *J. Am. Chem. Soc.* **1992**, *114*, 4983–4992.
- (48) The experimental difference in zero-point energies for TEMPO-H(D) in MeCN is estimated as  $0.5[\nu_{\text{OH}} - \nu_{\text{OD}}] = 452 \text{ cm}^{-1} = 1.3 \text{ kcal mol}^{-1}$ .

- (49) The KIEs are not sensitive to solvent even though the characteristic solvent reorganization times are about a factor of two longer for CH<sub>2</sub>Cl<sub>2</sub> than for MeCN: Hornig, M. L.; Gardecki, J. A.; Papazyan, A.; Maroncelli, M. *J. Phys. Chem.* **1995**, *99*, 17311.
- (50) (a) 'Bu<sub>2</sub>NO $\cdot$ ' is slightly more crowded than the cyclic analogs, as reflected in its slightly larger CNC angle of 129.6(3) $^\circ$  versus 123.5(2) $^\circ$  for 4-oxo-TEMPO $\cdot$ . Cotton, F. A.; Felthouse, T. R. *Inorg. Chem.* **1982**, *21*, 2667. Two molecules of 'Bu<sub>2</sub>NO $\cdot$ ' were co-crystallized with Rh<sub>2</sub>(O<sub>2</sub>CCF<sub>3</sub>)<sub>4</sub>(H<sub>2</sub>O)<sub>2</sub>. (b) Andersen, B.; Andersen, P. *Acta Chem. Scand.* **1966**, *20*, 2728.  $\angle\text{CNC} = 136(3)^\circ$  of 'Bu<sub>2</sub>NO $\cdot$ ' in the gas phase was determined by electron diffraction. (c) Bordeaux, P. D.; Lajzėrowicz, J. *Acta Crystallogr., Sect. B* **1974**, *30*, 790.

does not include hydrogen tunneling. Still, the cross relation is essentially interpretative, and will still hold if the self-exchange and cross reactions are accelerated a comparable amount by tunneling.

**III. Comparison with Related Reactions.** The rate constants for nitroxyl + hydroxylamine self-exchange and pseudo self-exchange reactions show a remarkable range, from 2 to  $>10^7$   $\text{M}^{-1} \text{s}^{-1}$  (Table 2). Other  $\text{XO}^* + \text{XOH}$  reactions show similar variation:  ${}^t\text{Bu}_2\text{C}=\text{NO}^* + {}^t\text{Bu}_2\text{C}=\text{NOH}$  in benzene,  $1.3 \text{ M}^{-1} \text{s}^{-1}$ ;  ${}^{53} 2,4,6\text{-}{}^t\text{Bu}_3\text{C}_6\text{H}_2\text{O}^* + 2,4,6\text{-}{}^t\text{Bu}_3\text{C}_6\text{D}_2\text{OH}$  in  $\text{CCl}_4$ ,  $220 \text{ M}^{-1} \text{s}^{-1}$ ;  ${}^{13b} {}^t\text{BuOO}^* + {}^t\text{BuOOH}$  in isopentane,  $490 \text{ M}^{-1} \text{s}^{-1}$ ;  ${}^{54} {}^t\text{BuO}^* + {}^t\text{Bu}_3\text{COH}$  in  ${}^t\text{BuOO}{}^t\text{Bu}$ ,  $\sim 3 \times 10^4 \text{ M}^{-1} \text{s}^{-1}$ ;  ${}^{55}$  and  $\text{PhO}^* + 2\text{-naphthol}$  ( $\Delta G^\circ \approx -2 \text{ kcal mol}^{-1}$ ) in MeCN,  $4.5 \times 10^6 \text{ M}^{-1} \text{s}^{-1}$ . ${}^{52,56}$  The most striking comparison is from the measurements of  $\text{R}_2\text{NOH} + \text{R}_2\text{NO}^*$  self-exchange reactions by Kreilick and Weissman in  $\text{CCl}_4$ :  $320 \text{ M}^{-1} \text{s}^{-1}$  for  $\text{R} = {}^t\text{Bu}$  vs  $>10^7 \text{ M}^{-1} \text{s}^{-1}$  for  $\text{R} = \text{Ph}$ . ${}^{13}$  The dichotomy between the dialkyl- and arylhydroxylamine reactions is also evident in the HAT kinetic isotope effects. The more rapid arylhydroxylamine reactions have  $k_{\text{H}}/k_{\text{D}} < 2$ , while the slower dialkylnitroxyl reactions have  $k_{\text{H}}/k_{\text{D}} > 10$  (Table 2).

Reactions of the acylnitroxyl PINO $^*$  display yet another pattern of reactivity. ${}^{17,18,39}$  The pseudo self-exchange reaction of PINO $^*$  with the hydroxyphthalate Me-NHPI has values of  $E_{\text{a}}$  ( $10 \text{ kcal mol}^{-1}$ ) and  $A_{\text{H}}$  ( $10^{10.4} \text{ M}^{-1} \text{s}^{-1}$ ) that are significantly larger than those of the TEMPO $^*/4\text{-oxo-TEMPO}^*/4\text{-MeO-TEMPO}^*$  reactions (eqs 2 and 3):  $E_{\text{a}} \leq 6 \text{ kcal mol}^{-1}$  and  $A_{\text{H}} \leq 10^5 \text{ M}^{-1} \text{s}^{-1}$  (Table 3). The reactions of PINO $^*$  with *p*-xylene and toluene appear to involve tunneling, but in contrast to reactions 2–4, they show large values of  $E_{\text{ad}} - E_{\text{aH}}$  and negative values of  $\log(A_{\text{H}}/A_{\text{D}})$  ( $3.0 \pm 0.3 \text{ kcal mol}^{-1}$ ,  $-0.8 \pm 0.3$  for *p*-xylene), suggesting that tunneling is more pronounced for H than for D. ${}^{17,18,39}$  The related HAT reaction of  $(\text{CF}_3)_2\text{NO}^*$  with toluene, with  $k_{\text{H}}/k_{\text{D}} = 13$  and  $\log(A_{\text{H}}/A_{\text{D}}) \approx 0$  ( $A_{\text{H}} \approx A_{\text{D}} \approx 10^4$ ), was not suggested to involve significant tunneling. ${}^{57}$

The diversity of behavior is remarkable for such similar reactions. All of the nitroxyl/hydroxylamine reactions discussed here are close to isoergic ( $\Delta\Delta G^\circ \leq 2 \text{ kcal mol}^{-1}$ , Table 2) so the driving forces are not the cause of these differences. The differences between the dialkyl- and the arylhydroxylamine reactions could conceivably be largely due to a steric effect. The bulkier tertiary alkyl groups might make assembly of the precursor complex more difficult and could keep the oxygen atoms farther apart. Such a difference in TS geometries would lead to higher barriers and longer H-transfer distances, enhancing

the importance of tunneling in the dialkylnitroxyl reactions. However, the results of our calculations show that there is very little difference between the geometries of the TSs for the dialkyl- and diarylnitroxyl self-exchange reactions. Instead, our calculations find that the much faster  $\text{Ph}_2\text{NO}^* + \text{Ph}_2\text{NOH}$  self-exchange reaction is due to the greater electronic delocalization provided by the phenyl groups in the transition structure. The CVT barrier for  $\text{Ph}_2\text{NO}^*/\text{H}$  self-exchange reaction,  $5.6 \text{ kcal mol}^{-1}$ , is 9–10  $\text{kcal mol}^{-1}$  lower than the CVT barriers for the  ${}^t\text{Bu}_2\text{NO}^*/\text{H}$  and TEMPO(H) self-exchange reactions (15.7, 14.5  $\text{kcal mol}^{-1}$ , respectively).

Because the reaction barriers for the arylhydroxylamines are lower than those for the dialkylhydroxylamines, the former reactions can proceed by passage over, or close to the top of the barriers, without the need for substantial tunneling. In contrast, the higher reaction barriers on the potential energy surfaces for the dialkylhydroxylamine reactions lead to both H and D preferentially tunneling through the barriers. Tunneling produces the low  $E_{\text{a}}$  and  $A$  values and the high H/D KIEs that we have both measured and calculated for the dialkylnitroxyl radical + dialkylhydroxylamine reactions.

While many discussions of tunneling emphasize the distance over which the H or D transfers must occur, in this case the O–H bond distances in the reactant complexes and transition structures are calculated to be quite similar for the reactions of dialkylhydroxylamines vs those of arylhydroxylamines. The results of our calculations suggest that the former reactions show the experimental indications of tunneling while the latter do not because of the different barrier heights for degenerate HAT in these two types of hydroxylamines. These studies thus appear to be an experimental example of the well-known theoretical result that barrier height is as key a factor as barrier width in determining the probability of tunneling in a chemical reaction. ${}^3$

## Conclusions

Hydrogen atom transfer from dialkylhydroxylamines to dialkylnitroxyl radicals predominantly involves hydrogen tunneling. This has been shown through a combination of experimental and computational studies. Experimentally, the kinetics of three pseudoself exchange reactions have been examined. For the reactions of 4-oxo-TEMPO $^*$  with TEMPO-H (eq 2) and 4-MeO-TEMPO-H (eq 3), the activation parameters and H/D kinetic isotope effects (Tables 2–4) suggest that tunneling is important in both H and D transfers. The measured ratios of  $k_{\text{H}}/k_{\text{D}} = 21\text{--}23 \pm 4$  correspond to intrinsic KIEs of ca. 40 at 298 K, given the  $98 \pm 1\%$  deuterium enrichment of the hydroxylamines. Computational studies of the  $(\text{CH}_3)_2\text{NO}^* + (\text{CH}_3)_2\text{NOH}$  model reaction, using the small-curvature tunneling (SCT) approximation, also find substantial tunneling by both H and D. The reaction of  ${}^t\text{Bu}_2\text{NO}^*$  with TEMPO-H (eq 4) has very unusual activation parameters, with  $E_{\text{a}}(\text{D}) < E_{\text{a}}(\text{H})$  and  $\log(A_{\text{H}}/A_{\text{D}}) \approx 3$ .

The properties of these pseudo self-exchange reactions of dialkylhydroxylamines contrast with related reactions of arylhydroxylamines. Aryl-substituted hydroxylamines generally react with higher rate constants and very small KIEs ( $<2$ ). Calculations indicate that the  $\text{Ph}_2\text{NO}^* + \text{Ph}_2\text{NOH}$  self-exchange has a 9–10  $\text{kcal mol}^{-1}$  lower barrier than the  ${}^t\text{Bu}_2\text{NO}^* + {}^t\text{Bu}_2\text{NOH}$  and TEMPO + TEMPO-H self-exchange reactions, due to greater electron delocalization in the  $[\text{Ph}_2\text{NO}\cdots\text{H}\cdots\text{ONPh}_2]^*$  transition structure. The picture that emerges from these studies is that the self-exchange reactions of the

- (51) (a)  $E_{\text{ad}} - E_{\text{aH}} = -2.8 \text{ kcal mol}^{-1}$  and  $\log(A_{\text{H}}/A_{\text{D}}) = 2.2$  have been reported for  $e^-/\text{H}^+$  from 2,3-dimethoxy-5-methyl-1,4-benzoquinol to the excited state of  $[\text{Ru}(2,2'\text{-bipyridine})_2\{2\text{-}(2\text{-pyridyl})\text{benzimidazole}\}^+]$ : Cape, J. L.; Bowman, M. K.; Kramer, D. M. *J. Am. Chem. Soc.* **2005**, *127*, 4208. (b) This result has very recently been rationalized in terms of being close to the Marcus inverted region for PCET: Ludlow, M. K.; Soudackov, A. V.; Hammes-Schiffer, S. *J. Am. Chem. Soc.* **2009**, *131*, 7094–7102. (c) HAT self-exchange between  $[\text{Fe}^{\text{II}}(\text{H}_2\text{bip})_3]^{2+}$  and  $[\text{Fe}^{\text{III}}(\text{H}_2\text{bip})_2(\text{Hbip})]^{2+}$  ( $\text{H}_2\text{bip} = 2,2'\text{-bi-1,4,5,6-tetrahydropyrimidine}$ ) also appears to have negative  $E_{\text{ad}} - E_{\text{aH}} = -1.2 \pm 0.8 \text{ kcal mol}^{-1}$  and positive  $\log(A_{\text{H}}/A_{\text{D}}) = 0.9 \pm 1.2$  values: Yoder, J. C.; Roth, J. P.; Gussenhoven, E. M.; Larsen, A. S.; Mayer, J. M. *J. Am. Chem. Soc.* **2003**, *125*, 2629.
- (52) Foti, M.; Ingold, K. U.; Luszyk, J. *J. Am. Chem. Soc.* **1994**, *116*, 9440.
- (53) Mendenhall, G. D.; Ingold, K. U. *J. Am. Chem. Soc.* **1973**, *95*, 627–628.
- (54) Chénier, J. H. B.; Howard, J. A. *Can. J. Chem.* **1975**, *53*, 623.
- (55) Griller, D.; Ingold, K. U. *J. Am. Chem. Soc.* **1974**, *96*, 630.
- (56) Bordwell, F. G.; Cheng, J. *J. Am. Chem. Soc.* **1991**, *113*, 1736.
- (57) (a) Doba, T.; Ingold, K. U. *J. Am. Chem. Soc.* **1984**, *106*, 3958. (b) Malatesta, V.; Ingold, K. U. *J. Am. Chem. Soc.* **1981**, *103*, 3094.



dialkylhydroxylamines involve tunneling of both H and D, while the related reactions of arylhydroxylamines proceed over or close to the top of the reaction barriers. This dichotomy is due to the higher barriers for the dialkylhydroxylamine reactions, rather than to differences in the geometries of the reactant complexes or transition structures between the two types of hydroxylamines.

## Experimental Section

**Physical Techniques and Instrumentation.**  $^1\text{H}$  (500 MHz) and  $^{13}\text{C}\{^1\text{H}\}$  (126 MHz) NMR were recorded on Bruker Avance spectrometers, referenced to a residual solvent peak, and reported as:  $\delta$  (multiplicity, assignment, number of protons). The error for NMR integration is estimated to be  $\pm 10\%$ . Lorentzian line fitting for accurate integration was done using NUTS.<sup>25</sup> Electrospray ionization mass spectra (ESI/MS) were obtained on a Bruker Esquire-LC ion trap mass spectrometer and reported as  $m/z$ , with samples infused as MeCN solutions. UV-vis spectra were acquired with a Hewlett-Packard 8453 diode array spectrophotometer, and reported as  $\lambda_{\text{max}}/\text{nm}$  ( $\epsilon/\text{M}^{-1}\text{cm}^{-1}$ ). IR spectra were obtained as  $\text{CD}_3\text{CN}$ ,  $\text{CD}_2\text{Cl}_2$ , or  $\text{CCl}_4$  solutions in a NaCl solution cell, using a Bruker Vector 33 or Perkin-Elmer 1720 FT-IR spectrometer, and reported in  $\text{cm}^{-1}$ . UV-vis stopped-flow measurements were obtained on an OLIS RSM-1000 stopped-flow spectrophotometer. Elemental analyses were performed by Atlantic Microlab (Norcross, GA). All reactions were performed in the absence of air using standard glovebox/vacuum line techniques.

**Materials.** All reagent grade solvents were purchased from Fisher Scientific, EMD Chemicals, or Honeywell Burdick & Jackson (for anhydrous MeCN). Deuterated solvents were obtained from Cambridge Isotope Laboratories.  $\text{CD}_3\text{CN}$  was dried over  $\text{CaH}_2$ , vacuum transferred to  $\text{P}_2\text{O}_5$ , and over to  $\text{CaH}_2$ , then to a dry glass flask.  $\text{CD}_2\text{Cl}_2$  was dried over  $\text{CaH}_2$ , and vacuum transferred to a dry glass flask. TEMPO, 4-oxo-TEMPO, 4-MeO-TEMPO, and  $^t\text{Bu}_2\text{NO}^{\cdot}$  were purchased from Aldrich, and were sublimed onto a coldfinger apparatus before use. UV-vis (MeCN): TEMPO, 460 (10.3); 4-oxo-TEMPO, 440 (5.5); 4-MeO-TEMPO, 460 (10.4);  $^t\text{Bu}_2\text{NO}^{\cdot}$ , 454 (8.9). UV-vis ( $\text{CH}_2\text{Cl}_2$ ): TEMPO, 460 (11.1); 4-oxo-TEMPO, 446 (6.0); 4-MeO-TEMPO, 462 (11.0);  $^t\text{Bu}_2\text{NO}^{\cdot}$ , 450 (9.0). UV-vis ( $\text{CCl}_4$ ): TEMPO, 471 (12.2); 4-oxo-TEMPO, 450 (7.1). Anal. Calcd (Found) for TEMPO ( $\text{C}_9\text{H}_{18}\text{NO}$ ): C, 69.18 (69.14); H, 11.61 (11.65); N, 8.96 (9.09); for 4-oxo-TEMPO ( $\text{C}_9\text{H}_{16}\text{NO}_2$ ): C, 63.50 (63.61); H, 9.47 (9.51); N, 8.23 (8.19); for 4-MeO-TEMPO ( $\text{C}_{10}\text{H}_{20}\text{NO}_2$ ): C, 64.48 (64.64); H, 10.82 (10.97); N, 7.52 (7.47); for  $^t\text{Bu}_2\text{NO}^{\cdot}$  ( $\text{C}_8\text{H}_{18}\text{NO}$ ): C, 66.62 (66.87); H, 12.58 (12.79); N, 9.71 (9.61).

TEMPO-H was prepared according to literature procedures.<sup>23a,58</sup>  $^1\text{H}$  NMR ( $\text{CD}_3\text{CN}$ ):  $\delta$  1.06 (s,  $\text{CH}_3$ , 12H), 1.45 (s,  $\text{CH}_2$ , 6H); the C3/C5 and C4 signals are coincident), 5.34 (br s, OH, 1H).  $^1\text{H}$  NMR ( $\text{CD}_2\text{Cl}_2$ ):  $\delta$  1.10 (s,  $\text{CH}_3$ , 12H), 1.46 (s,  $\text{CH}_2$ , 6H), 4.31 (br s, OH, 1H).  $^{13}\text{C}\{^1\text{H}\}$  NMR ( $\text{CD}_3\text{CN}$ ):  $\delta$  17.78 (C4), 26.11 ( $\text{CH}_3$ ), 40.16 (C3), 58.78 (C2). Anal. Calcd (Found) for TEMPO-H ( $\text{C}_9\text{H}_{19}\text{NO}$ ): C, 68.74 (69.01); H, 12.18 (12.39); N, 8.91 (8.82). TEMPO-D was prepared analogously to TEMPO-H, using  $(\text{CD}_3)_2\text{CO}/\text{D}_2\text{O}$  (99.9% D in  $\text{D}_2\text{O}$ ) as the solvent; it was  $98 \pm 1\%$  OD by NMR integration. Anal. Calcd (Found) for TEMPO-D ( $\text{C}_9\text{H}_{18}\text{DNO}$ ): C, 68.30 (67.42); H, 12.10 (12.21); N, 8.85 (8.68). IR:  $\nu_{\text{OH}}/\nu_{\text{OD}} = 3495/2592$  ( $\text{CD}_3\text{CN}$ ), 3583/2648 ( $\text{CD}_2\text{Cl}_2$ ), 3597/2658 ( $\text{CCl}_4$ ).

**Preparation of 4-MeO-TEMPO-H.** A suspension of 4-MeO-TEMPO $^{\cdot}$  (2.00 g, 10.7 mmol) and  $\text{Na}_2\text{S}_2\text{O}_4$  (3.60 g, 20.7 mmol) in  $\text{Me}_2\text{CO}/\text{H}_2\text{O}$  (15 mL each) was stirred for 30 min at room temperature under  $\text{N}_2$ . The solvent was then partially evacuated under vacuum to remove  $\text{Me}_2\text{CO}$ . The leftover aqueous layer was extracted with  $\text{Et}_2\text{O}$  ( $3 \times 20$  mL), and the solvent was evacuated to dryness to give the crude product, which was purified by sublimation to a coldfinger, yielding 951 mg of white powder

(48%).  $^1\text{H}$  NMR ( $\text{CD}_3\text{CN}$ ):  $\delta$  1.09, 1.10 (s,  $\text{CH}_3$ , 6H each); 1.25, 1.90 (m,  $\text{CH}_2$ , 2H each); 3.25 (s,  $\text{OCH}_3$ , 3H); 3.46 (m, 4-CH, 1H); 5.37 (br s, OH, 1H).  $^1\text{H}$  NMR ( $\text{CD}_2\text{Cl}_2$ ):  $\delta$  1.16, 1.20 (s,  $\text{CH}_3$ , 6H each); 1.33, 1.90 (m,  $\text{CH}_2$ , 2H each); 3.32 (s,  $\text{OCH}_3$ , 3H); 3.44 (m, 4-CH, 1H); 4.51 (br s, OH, 1H).  $^{13}\text{C}\{^1\text{H}\}$  NMR ( $\text{CD}_3\text{CN}$ ):  $\delta$  20.83, 32.74 ( $\text{CH}_3$ ); 45.25 (C3); 55.77 ( $\text{OCH}_3$ ); 59.22 (C2); 72.57 (C4). ESI/MS $^+$ : 188 [ $\text{M} + \text{H}$ ] $^+$ , 170 [ $\text{M} - \text{OH}$ ] $^+$ . Anal. Calcd (Found) for 4-MeO-TEMPO-H ( $\text{C}_{10}\text{H}_{21}\text{NO}_2$ ): C, 64.13 (64.28); H, 11.30 (11.31); N, 7.48 (7.49). 4-MeO-TEMPO-D was prepared analogously using  $(\text{CD}_3)_2\text{CO}/\text{D}_2\text{O}$  (99.9% D in  $\text{D}_2\text{O}$ ) and was  $98 \pm 1\%$  OD by NMR integration. Anal. Calcd (Found) for 4-MeO-TEMPO-D ( $\text{C}_{10}\text{H}_{20}\text{DNO}_2$ ): C, 63.79 (63.92); H, 11.24 (11.37); N, 7.44 (7.55). IR ( $\text{CD}_3\text{CN}$ ):  $\nu_{\text{OH}}/\nu_{\text{OD}} = 3492/2584$ .

**$^1\text{H}$  NMR Equilibrium Measurements.** A typical experiment involved a J-Young sealable NMR tube being loaded with 4-oxo-TEMPO $^{\cdot}$  (48 mg, 0.28 mmol) and TEMPO-H(D) (76 mg, 0.48 mmol) in 0.5 mL  $\text{CD}_3\text{CN}$  or  $\text{CD}_2\text{Cl}_2$  to form an equilibrium mixture with 4-oxo-TEMPO-H(D) and TEMPO $^{\cdot}$ .  $^1\text{H}$  NMR spectra of the sample were obtained at 278–318 K. All chemical species have resolvable peaks, whose integrations were determined by Lorentzian line fitting using NUTS.<sup>25</sup> An equilibrium constant was calculated at each temperature from the ratios of the peak areas, corrected for the number of protons for each peak. The experiment was repeated with 4-oxo-TEMPO $^{\cdot}$ /TEMPO-H(D) = 32 mg/51 mg, and 24 mg/38 mg and the reported  $K$  at each temperature is the average of three runs. The errors on  $K$  are  $2\sigma$  of the variation of measured values. The errors on  $\Delta H^\circ$  and  $\Delta S^\circ$  are  $2\sigma$  errors from the least-squares linear fit using KaleidaGraph<sup>59</sup> to the van't Hoff equation.

$^1\text{H}$  NMR of TEMPO $^{\cdot}$  in  $\text{CD}_3\text{CN}$ :  $-\delta$  29.74 (3,5- $\text{CH}_2$ , 4H),  $-\delta$  16.51 ( $\text{CH}_3$ , 12H), 15.33 (4- $\text{CH}_2$ , 2H); in  $\text{CD}_2\text{Cl}_2$ :  $-\delta$  27.97 (3,5- $\text{CH}_2$ , 4H),  $-\delta$  15.14 ( $\text{CH}_3$ , 12H), 15.19 (4- $\text{CH}_2$ , 2H).  $^1\text{H}$  NMR of 4-oxo-TEMPO $^{\cdot}$  in  $\text{CD}_3\text{CN}$ :  $-\delta$  7.78 ( $\text{CH}_3$ , 12H), 1.80 (3,5- $\text{CH}_2$ , broad, 4H, overlaps with residual solvent [ $\text{CH}_2\text{DCN}$ ] peak); in  $\text{CD}_2\text{Cl}_2$ :  $-\delta$  7.12 ( $\text{CH}_3$ , 12H), 2.22 (3,5- $\text{CH}_2$ , 4H).  $^1\text{H}$  NMR of 4-MeO-TEMPO $^{\cdot}$  in  $\text{CD}_3\text{CN}$ :  $-\delta$  33.89,  $-\delta$  20.42 (3,5- $\text{CH}_2$ , 2H each);  $-\delta$  29.43,  $-\delta$  1.74 ( $\text{CH}_3$ , 6H each); 3.07 ( $\text{OCH}_3$ , 3H); 8.67 (4-CH, 1H).  $^1\text{H}$  NMR of  $^t\text{Bu}_2\text{NO}^{\cdot}$  (s,  $^t\text{Bu}$ ) in  $\text{CD}_3\text{CN}$ :  $-\delta$  6.67; in  $\text{CD}_2\text{Cl}_2$ :  $-\delta$  6.20. 4-oxo-TEMPO-H and  $^t\text{Bu}_2\text{NOH}$  were not isolated but were generated *in situ* in reactions 2 and 4, respectively.  $^1\text{H}$  NMR of 4-oxo-TEMPO-H in  $\text{CD}_3\text{CN}$ : 1.22 (s,  $\text{CH}_3$ , 12H); 2.39 (s,  $\text{CH}_2$ , 4H); in  $\text{CD}_2\text{Cl}_2$ : 1.24 (s,  $\text{CH}_3$ , 12H); 2.49 (s,  $\text{CH}_2$ , 4H).  $^1\text{H}$  NMR of  $^t\text{Bu}_2\text{NOH}$  (s,  $^t\text{Bu}$ ) in  $\text{CD}_3\text{CN}$ : 1.23; in  $\text{CD}_2\text{Cl}_2$ : 1.31.

**UV-Vis Stopped-Flow Kinetic Measurements.** Solutions of 4-oxo-TEMPO $^{\cdot}$  (12–24 mM) and TEMPO-H(D) (118–584 mM) in MeCN or  $\text{CH}_2\text{Cl}_2$  were prepared and loaded into gastight syringes inside a  $\text{N}_2$  glovebox. The stopped-flow apparatus was flushed with the solvent, and a background spectrum was acquired. The syringes were immediately loaded onto the stopped-flow apparatus to minimize air exposure. The stopped-flow drive syringes were flushed with the reagents, then filled and allowed to thermally equilibrate. A minimum of six kinetic runs were performed for each set of concentrations at 278–318 K in MeCN or at 273–308 K in  $\text{CH}_2\text{Cl}_2$  for reaction 2. The contents of the two syringes were rapidly mixed at equal volume resulting in half of the original concentrations (5.9–12 mM 4-oxo-TEMPO $^{\cdot}$  and 59–292 mM TEMPO-D). Kinetic data were analyzed using SPECFIT global analysis software<sup>28</sup> to determine the rate constants. Under pseudofirst order conditions ( $\geq 10$  equiv TEMPO-H(D)),  $k_{\text{obs}}$  values were derived from fitting an  $\text{A} \rightarrow \text{B}$  model at each [TEMPO-H(D)], and second order rate constants were obtained from plotting  $k_{\text{obs}}$  versus [TEMPO-H(D)] (Figure 3). Under second order conditions, the data were fit to an opposing second order equilibrium model,  $\text{A} + \text{B} \rightleftharpoons \text{C} + \text{D}$  (A and C colored), with a fixed equilibrium constant (Table 1). Reaction 2 was also performed in  $\text{CCl}_4$  at 298 K under pseudofirst order conditions ( $\geq 10$  equiv TEMPO-H(D)). Temperature dependent measurements of reaction 3 used similar amounts of 4-oxo-TEMPO $^{\cdot}$  and 4-MeO-TEMPO-H(D) in MeCN; for reac-

(58) Ozinskas, A. J.; Bobst, A. M. *Helv. Chim. Acta* **1980**, *63*, 1407.

(59) KaleidaGraph, version 3.5; Synergy Software Reading, PA, 2000.



tion 4, 12–139 mM 'Bu<sub>2</sub>NO' and 118–237 mM TEMPO-H(D) in MeCN or CH<sub>2</sub>Cl<sub>2</sub> were used (as the initial concentrations right after stopped-flow mixing). The errors on  $k$  are  $2\sigma$  of the variation of measured values. The errors on the activation parameters are  $2\sigma$  from the least-squares linear fit using KaleidaGraph<sup>59</sup> to the Eyring or Arrhenius equation.

**Acknowledgment.** We thank J. J. Warren for insightful discussions and the US National Institutes of Health (GM50422) and the University of Washington for financial support. The research at the University of North Texas was supported by the National Science and Robert A. Welch Foundations. Some of the results reported here were obtained on computers, purchased with funds provided by the National Science Foundation under grant CHE-

0741936. E.A.M. gratefully acknowledges funding from the Natural Science and Engineering Research Council of Canada (NSERC PGS D2).

**Supporting Information Available:** Figures S1–S3, the complete author lists for refs 32 and 33, the optimized geometries, energies, frequencies, and thermal corrections for nitroxyl radicals (RR'NO'), hydroxylamines (RR'NOH), and their hydrogen bonded complexes and hydrogen atom transfer transition structures, for R = R' = Me, R = H/R' = Me, R = R' = 'butyl, R = R' = phenyl, and TEMPO'. This material is available free of charge via the Internet at <http://pubs.acs.org>.

JA904400D